Osmotic surveillance mediates rapid wound closure through nucleotide release

William J. Gault, Balázs Enyedi, and Philipp Niethammer

Cell Biology Program, Memorial Sloan Kettering Cancer Center, New York, NY 10065

Osmotic cues from the environment mediate rapid detection of epithelial breaches by leukocytes in larval zebrafish tail fins. Using intravital luminescence and fluorescence microscopy, we now show that osmolarity differences between the interstitial fluid and the external environment trigger ATP release at tail fin wounds to initiate rapid wound closure through long-range activation of basal epithelial cell motility. Extracellular nucleotide breakdown, at least in part mediated by ecto-nucleoside triphosphate diphosphohydrolase 3 (*Entpd3*), restricts the range and duration of osmotically induced cell migration after injury. Thus, in zebrafish larvae, wound repair is driven by an autoregulatory circuit that generates pro-migratory tissue signals as a function of environmental exposure of the inside of the tissue.

Introduction

Rapid epithelial wound closure is essential for metazoan life, as it restricts exposure of the inside of an organism to the noxious outside environment. Wound closure mechanisms operate efficiently in animals that occupy different habitats (e.g., land/river/sea), and whose epithelia are exposed to vastly different physicochemical environments (air, fresh/salt water, etc.). Wound closure shows striking similarities to morphogenetic processes, such as dorsal closure in *Drosophila melanogaster* (Redd et al., 2004). These developmental events are thought to be regulated by organism-intrinsic cues; i.e., the external environment does not instruct them. Given its robust functionality throughout phyla, and analogy to developmental mechanisms, it is intuitive (and in fact common) to regard wound repair as an intrinsically guided, postdevelopmental program. Yet, it remains unclear whether the conserved function of wound repair derives from an insulation against extrinsic influences, or an adaption to them. The question arises whether epithelial wound detection and repair are obligatory tissue-intrinsic processes, or if they also integrate information from the environment.

Zebrafish is a powerful system to study wound responses and their possible environmental adaption in the intact animal (Redd et al., 2004; Huttenlocher and Poznansky, 2008; Richardson et al., 2013). The tail fin fold of 2–4-d-old zebrafish larvae is a double-layered epithelium consisting of a basal epithelial layer that is attached to a basal lamina, and a suprabasal layer in which cells are connected by adherens and tight junctions (Fig. 1 a; Sonawane et al., 2009). This stratified skin fold protects the inside of the zebrafish ($\sim$270–300 mOsm, i.e., common vertebrate extracellular tonicity) from its natural hypotonic freshwater environment ($\sim$10 mOsm), analogous to the stratified linings of mouth and esophagus, which protect mammalian tissues from hypotonic saliva ($\sim$30 mOsm). The thinness and transparency of zebrafish tail fins facilitates interrogation of tissue damage detection mechanisms through pharmacologic/genetic perturbations and intravital microscopy. Using the zebrafish tail fin wounding assay, we previously demonstrated that a drop in interstitial osmotic pressure initiates eicosanoid-mediated leukocyte recruitment (Enyedi et al., 2013). In the present study, we asked whether osmotic signaling is an environmental master regulator of wound responses by examining its potential involvement in epithelial repair.

Results

Environmental hypotonicity triggers rapid wound closure in zebrafish larvae

To test for a role of external tonicity, we imaged wound closure in larval zebrafish tail fins after UV laser wounding of fish

Correspondence to Philipp Niethammer: niethamp@mskcc.org

The Rockefeller University Press $30.00
J. Cell Biol. Vol. 207 No. 6   767–782
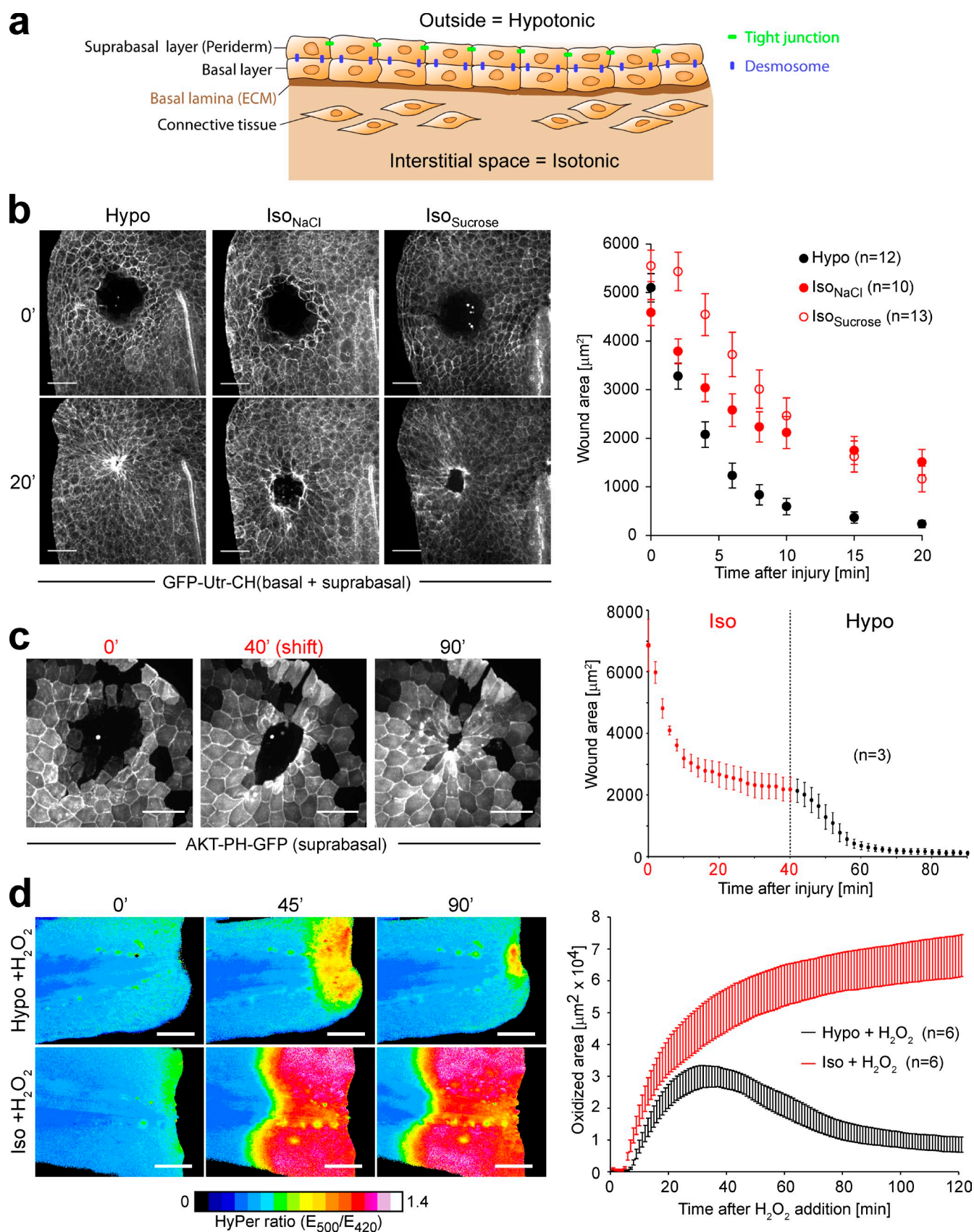www.jcb.org/cgi/doi/10.1083/jcb.201408049

JCB   **767**

Figure 1.   A transepithelial osmotic pressure gradient is required for rapid wound closure and barrier reconstitution of zebrafish tail fin wounds. (a) Simplified scheme of larval zebrafish tail fin epithelium ~3 dpf. Putative cell–cell contacts are indicated. (b, left) Representative time-lapse montage of zebrafish larvae immersed in hypotonic (Hypo) or isotonic (Iso$_{NaCl}$, Iso$_{Sucrose}$) solutions at the indicated times after UV laser puncture injury. The actin cytoskeleton is labeled with GFP-Utr-CH. Bars, 50 μm. (b, right) Quantification of wound area as a function of time after injury. (c, left) Time-lapse montage of suprabasal

immersed in either normal, hypotonic bathing medium or bathing medium that had been adjusted to the ionic composition and/or tonicity of vertebrate interstitial fluid (with the addition of NaCl or sucrose). The actin cytoskeleton and plasma membranes were labeled using GFP-utrophin-calponin homology domain (GFP-Utr-CH; Burkel et al., 2007), and AKT-pleckstrin homology domain (AKT-PH)–GFP (Kwon et al., 2007), respectively. Injection of mRNA into one-cell stage embryos led to ubiquitous labeling. In contrast, injection at the 4–8-cell stage gave rise to mosaic labeling of predominantly basal epithelial cells (Fig. S1 a). Basal epithelial cell labeling was also performed by injection of DNA constructs containing a fluorescent protein under the control of a basal cell–specific $\Delta Np63$ promoter (Reischauer et al., 2009). Suprabasal labeling was achieved by expression via a keratin promoter (Gong et al., 2002). Several pulses of a micropoint laser (435 nm) were used to produce wounds on both sides of the epithelial fold. Importantly, these full-thickness wounds are unlikely to close by contraction of underlying structures, because those are ablated by the laser blast. In hypotonic fish bathing solution (standard E3 medium), closure of $\sim$5,000-μm^2 puncture wounds was completed within $\sim$20 min, i.e., $\sim$5× faster than closure of similar sized lesions in *Drosophila* larvae (Geiger et al., 2011). Isotonicity (Iso$_{NaCl}$ or Iso$_{Sucrose}$) inhibited wound closure, with NaCl showing a more pronounced inhibition (Fig. 1 b and Video 1). Isotonic inhibition of wound closure was reversible (Fig. 1 c and Video 2). We also tested whether isotonicity blocks restoration of barrier function. To this end, we amputated the tail fin tips of transgenic zebrafish larvae ubiquitously expressing a genetically encoded, reversible fluorescent H_2O_2 reporter (HyPer; Belousov et al., 2006) in isotonic medium. After the endogenous, injury-induced HyPer signal (Niethammer et al., 2009) had subsided, the *Tg(actb2:HyPer)* transgenic fish were mounted in isotonic agarose and overlaid with isotonic or hypotonic solution supplemented with H_2O_2. Intact tail fin skin is impermeable to both H_2O and H_2O_2. H_2O_2 in the bathing solution probes wound permeability by eliciting a HyPer signal upon entering the fish. This signal was sustained upon isotonic, but not hypotonic, bath exposure, which is consistent with delayed barrier recovery in isotonic solution (Fig. 1 d and Video 3). Similar to the initial inflammatory response (Enyedi et al., 2013), rapid repair of zebrafish tail fin wounds depends on the osmotic difference between the freshwater environment and the interstitial fluid of the fish.

Environmental hypotonicity triggers migration of basal epithelial cells

Wound margin contraction through an actin cable (Martin and Lewis, 1992; Bement et al., 1993) or epithelial cell migration are the most plausible mechanisms for rapid wound closure in our model (see Discussion). To experimentally define the processes

underlying isotonic inhibition of closure, we imaged the morphological responses of epithelial cells by expressing fluorescent markers for actin, myosin, and plasma membrane in different epithelial layers. Time-lapse videos revealed rapid formation of lamellipodia in the basal, but not the suprabasal, layer after injury in hypotonic solution (Fig. 2, a and b; Fig. 3 a; and Video 4). Notably, migrating cells that had arrived at the wound margin abruptly ceased migration, and underwent a drastic morphological change that involved cell rounding, apparent shrinkage, and extension of phosphatidylinositol (3,4,5)-trisphosphate (PIP3)-positive fingerlike protrusions (Fig. 2 a and Video 4). By terminating cell migration at the cell margin, and making room for subsequent rows of cells (through compaction of wound margin cells), this process may contribute to the orderly and sequential advancement of migrating basal cells toward the wound. Propagation of lamellipodia formation distal to the wound was strongly inhibited by isotonicity (Iso$_{NaCl}$ or Iso$_{Sucrose}$), with NaCl having a slightly more pronounced effect (Fig. 3 a and Fig. S1 b). Suppression of lamellipodia formation by isotonicity or cytochalasin D was paralleled by inhibition of basal cell translocation (Fig. 3 b) and wound closure (Fig. S2 a). Both the morphological transition of basal cells (see above) to a rounded shape at the wound margin and the propagated wave of basal cell crawling were absent in isotonic wounds, while fingerlike protrusions positive for PIP3 could be observed at the basal cell margin.

We could detect recruitment of actin and myosin II at the wound margin by imaging ubiquitously expressed GFP-Utr-CH (Fig. 1 b) and mKate2-labeled myosin regulatory light chain (MRLC-mKate2; Fig. 3 c), or suprabasally expressed GFP-Utr-CH (Fig. S1 c). Together, these data indicate the formation of a "purse string" (Martin and Lewis, 1992; Bement et al., 1993) in the suprabasal layer. We cannot formally exclude purse string formation in the basal epithelial sheet, but our experiments do not bear evidence for it. Unlike at the rounded suprabasal margin (Fig. 2 a, white arrow; and Video 4), fingerlike protrusions appear to predominate at the basal wound margin as mentioned above (Fig. 2 a, yellow arrow; and Video 4). Actin and myosin recruitment to the wound margin seemed little affected by tonicity (Figs. 1 b and 3 c). Likewise, wound margin rounding, which is indicative of a functional purse string, was visible in isotonicity (Fig. 1, b and c; and Videos 1 and 2). Thus, spatially separated wound closure mechanisms (i.e., suprabasal purse string contraction and basal cell migration) mediate rapid wound closure in zebrafish larvae.

Morphodynamic profiling of epithelial sheet motion by particle image velocimetry (PIV)

Wound area assays (e.g., Fig. 1 b) integrate the functional contributions of all force-generative processes operant in an injured

AKT-PH-GFP (plasma membrane PIP3) expressing zebrafish larvae wounded and incubated in isotonic mounting agar (0′–40′), and overlaid with hypotonic fish bathing solution (40′–90′). Bars, 50 µm. (c, right) Quantification of wound area as a function of time after injury. Red indices, isotonic conditions. (d, left) Representative time-lapse montage of *Tg(actb2:HyPer)* larvae subjected to 1 mM H_2O_2 in hypotonic or isotonic bathing medium 1 h after tail fin tip amputation in isotonic bathing medium. The HyPer probe is reversibly oxidized by H_2O_2 that enters the fish through the wound, increasing the HyPer (E500/E420) emission ratio and probing for wound permeability as a function of time after injury. HyPer emission ratios are color-coded. Bars, 100 µm. (d, right) Quantification of oxidized tissue area as defined by high HyPer ratios (>0.64). Error bars indicate SEM of indicated (*n*) number of larvae. See Videos 1–3.
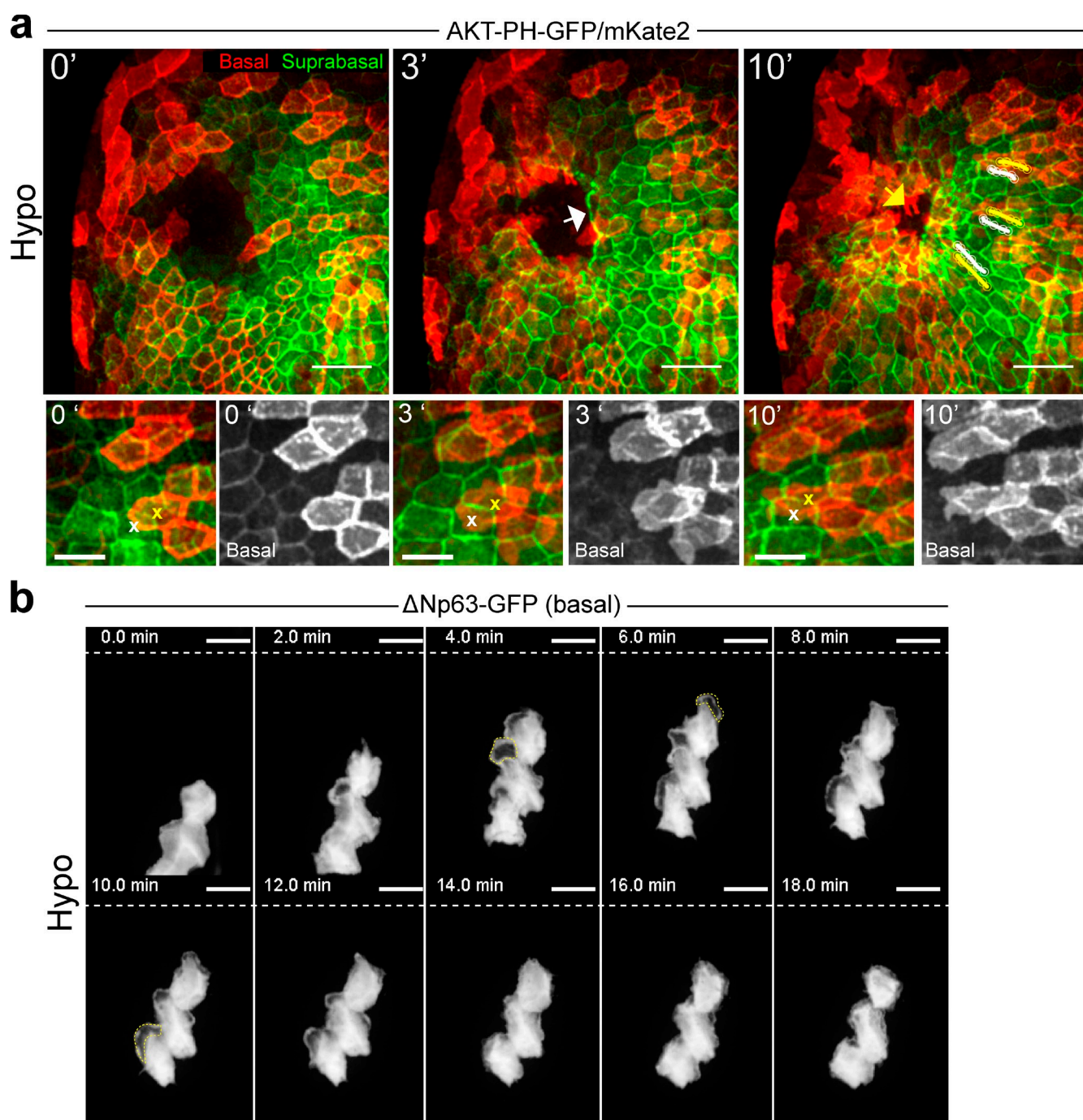
Figure 2. **Epithelial cell layers within the larval zebrafish epidermis exhibit distinct morphological wound closure mechanisms.** (a) Time-lapse images of a representative 2.5–3-dpf zebrafish larva at the indicated times after UV laser–induced injury. (a, top) Transgenic *Tg(krt4:AKT-PH-GFP)* expression of AKT-PH-GFP driven in the suprabasal cell layer (green) is observed simultaneously with mosaic AKT-PH-mKate2 in underlying basal epidermal cells (4–8-cell-stage mRNA injection; red) after puncture wounding in hypotonic E3 medium. Basal cells form lamellipodia and translocate collectively toward the wound, whereas the suprabasal cells translocate and elongate without visible lamellipodia. Note that basal cells at the margin can protrude across the wound opening (yellow arrow), whereas suprabasal cells at the margin align to form a smooth wound edge indicative of contractile "purse string" closure (white arrow). Basal and suprabasal cells maintain a largely consistent proximity; representative center of mass tracks for basal (yellow) and suprabasal (white) cells are shown (10', top right panel). Bars, 50 µm. (a, bottom) Enlargement of a region in the top panel; basal cell (yellow x) and neighboring suprabasal cell (white x) correspond to upper tracks in top right panel. Bars, 25 µm. All images are from a partial z projection to capture an individual epidermal bilayer. See Video 4. (b) Representative images of a 2.5–3-dpf zebrafish larva mosaically expressing GFP under the control of a basal cell–specific *ΔNp63* promoter, immersed in hypotonic bathing solutions shown at indicated times after UV laser cut injury. Broken white line, position of wound. Broken yellow lines, outlines of representative lamellipodial protrusions. Bars, 25 µm.

tissue, and their spatial coordination, as well as their mutual interactions into a single endpoint measurement. To obtain more specific information about the mechanisms that initiate cell motility in response to hypotonic exposure, we decided to directly measure wound-induced epithelial sheet motility by PIV analysis of the suprabasal layer (Fig. 4 a).
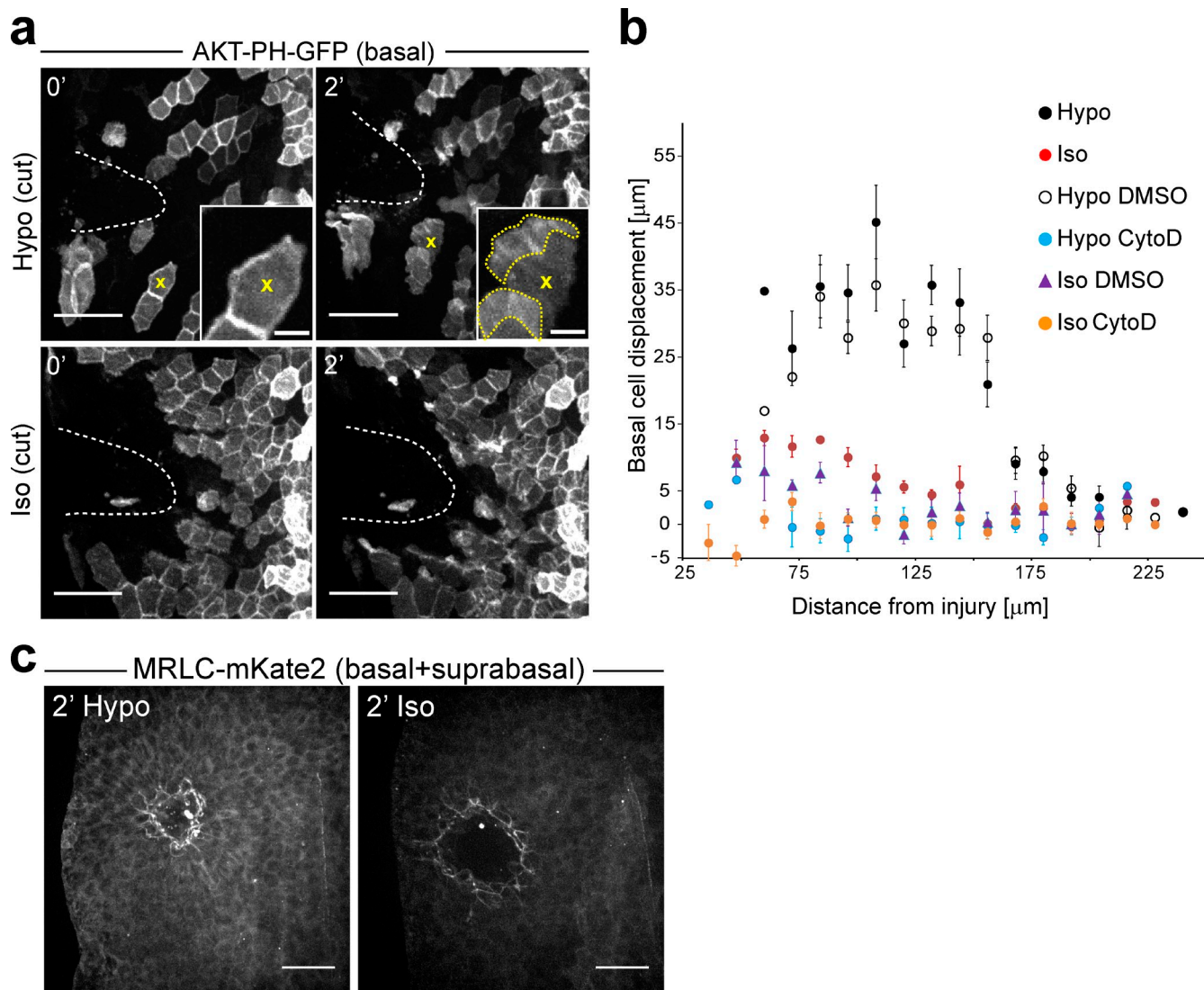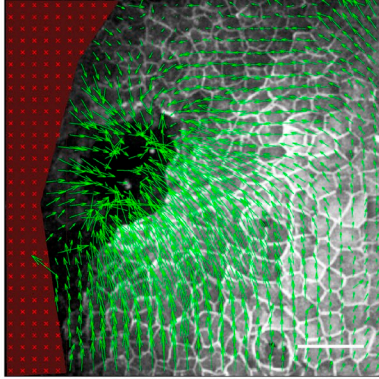
Figure 3. A drop in interstitial osmotic pressure after injury stimulates basal cell migration. (a) Representative images of 2.5–3-dpf zebrafish larvae mosaically expressing AKT-PH-GFP in basal cells (4–8-cell-stage mRNA injection), immersed in hypotonic or isotonic bathing solutions at the indicated times after UV laser cut injury. Broken white lines, wound margin. Yellow x, representative cell developing a lamellipodium (yellow dotted line) in response to a wound-induced exposure to hypotonicity. (b) Quantification of basal cell migration in zebrafish larvae mosaically labeled by one-cell stage *actb2*:Akt-PH-GFP DNA injections. Cell migration was tracked for ∼19 min after wounding in hypotonic medium (Hypo), isotonic medium (Iso), and hypotonic medium supplemented with 100 μM cytochalasin D (Hypo CytoD) to probe actin-dependent motility, DMSO control (Hypo DMSO), isotonic medium supplemented with 100 μM cytochalasin D (Iso CytoD), or Iso DMSO control (Iso DMSO). Mean basal cell displacement as a function of initial distance to the wound is shown for n = 123 cells/8 tail fins (Hypo), 114 cells/8 tail fins (Iso), 62 cells/5 tail fins (Hypo DMSO), 86 cells/6 tail fins (Hypo Cyto D), 79 cells/7 tail fins (Iso DMSO), and 122 cells/8 tail fins (Iso CytoD). Error bars indicate SEM. (c) Representative images of myosin II recruitment 2 min after UV-puncture injury in hypotonic (left) or isotonic (right) medium. Myosin recruitment is visualized by mKate2-labeled myosin regulatory light chain (one-cell stage mRNA injection). Bars: (a, main panels) 50 μm; (a, insets) 10 μm; (c) 50 μm.

Tissue velocity was measured as a function of time after injury (global PIV; Fig. 4 b) and/or distance from the wound (spatial PIV; Fig. 4 c). Averaging the motion profiles of multiple animals permitted quantitative comparison of dynamic "tissue-motion phenotypes" after experimental perturbations. Spatial PIV revealed that tissue motion spreads ∼150–200 μm away from the wound after hypotonic injury (Fig. 4 c), which is consistent with the length scale of basal cell translocation (Fig. 3 b). Highlighting statistical significant differences by subtracting hypotonic and isotonic velocity maps (Fig. 4 c) showed that isotonicity reduced amplitude and spatiotemporal spreading of motion through the tissue, in line with our

morphological observations. Some residual motion remained after isotonic injury (Fig. 4 b, red curve), which was further suppressed by preincubation with the Rho kinase inhibitor Y27632 (Fig. 4 b, green curve), a compound known to abrogate purse string formation (Abreu-Blanco et al., 2011). Interestingly, Y27632 prolonged sheet motion after hypotonic but not isotonic injury (Fig. 4 b, compare blue and gray curves), and appeared to interfere with coordination of tissue movements, at least to some degree. Specifically, closure movements appeared less regular, and not as concentrically balanced around the wound as in the control (Video 5). However, it remains unclear whether this effect is caused by the abrogation of the
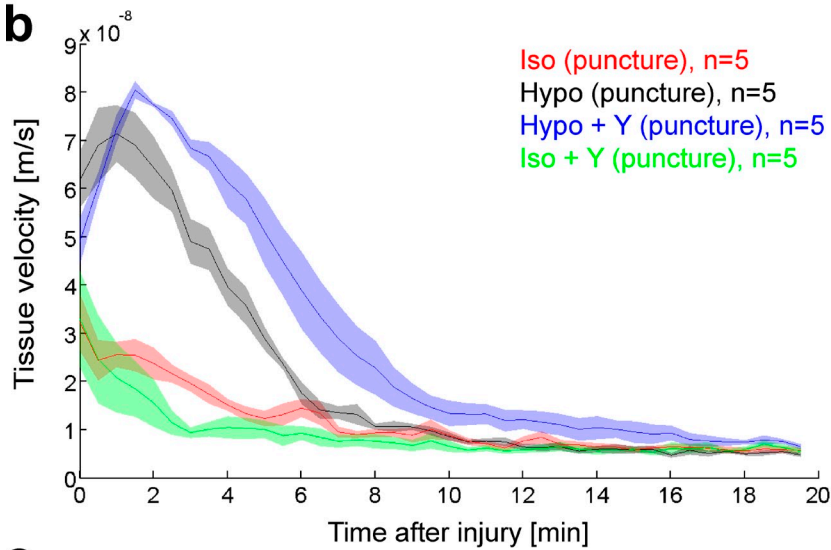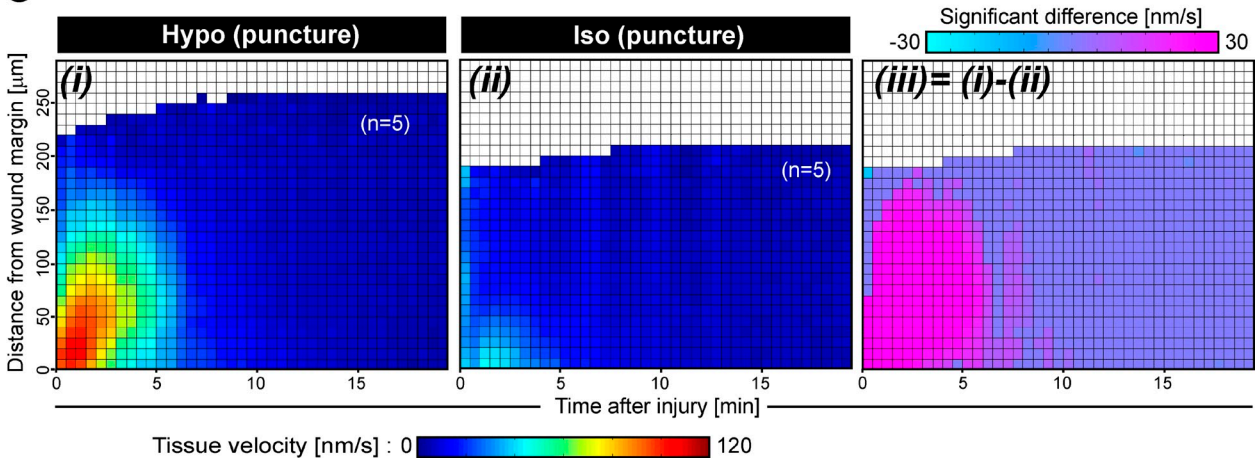
Figure 4. **Quantitative analysis of wound-induced epithelial sheet movement by PIV.** (a) Representative example of PIV analysis (PIVlab, MATLAB) of epithelial sheet movement after UV puncture injury of a *Tg(krt4:AKT-PH-GFP)* larva exhibiting plasma membrane labeling in the suprabasal layer. Green arrows, velocity vectors derived by comparing particle movements between subsequent frames. Red area, extra-tissue area excluded from analysis. Bar, 50 µm. (b) Global PIV analysis of UV-puncture wounded *Tg(krt4:AKT-PH-GFP)* larvae immersed in solutions of indicated composition (Y = Y27632, Rho-kinase inhibitor, 100 µM). The graph displays the mean of all velocity vector magnitudes within the unmasked field of view as a function of time after injury. (c) Spatial PIV analysis representing the Iso and Hypo datasets from b as spatially resolved 3D plots. (i and ii) Averaged spatial PIV plots of the indicated number of *Tg(krt4:AKT-PH-GFP)* larvae after UV-laser puncture injury in hypotonic or isotonic medium. Tissue velocities are color-coded (blue to green to yellow to red), and represented as a function of time after injury (x axis) and distance from injury site (y axis). (iii) Differential plot derived by subtraction of the indicated velocimetry plots, and *t* test filtering of statistically significant differences between groups (unpaired *t* test, P < 0.05 = significant difference). Statistically significant velocity differences are color-coded (turquoise to pink). Pink, positive values. Turquoise, negative values.

purse string, or decreased tissue tension in general. The fact that lamellipodial cell migration occurs only in the basal layer, but that motion is detected in the suprabasal layer even when the purse string is inhibited, suggests that the layers are mechanically coupled (e.g., desmosomes; Fig. 1 a; Sonawane et al., 2009) and that movement is largely promoted by the basal cells (Fig. S2 b). Supportive of this idea, basal and superficial cells maintain relative positions during movement (Fig. 2 a and Video 4). We therefore conclude that the superficial layer is dragged toward the wound primarily by osmotically induced basal cell migration, and potentially assisted (e.g., through spatial coordination) by an intrinsically triggered purse string contraction of the suprabasal wound margin.

Environmental hypotonicity stimulates wound-induced ATP release

Next, we investigated the mediators of basal cell migration after hypotonic injury. We previously showed that osmotically induced arachidonic acid release stimulates leukocyte migration to tail fin wounds (Enyedi et al., 2013). Arachidonic acid produced sporadic increases in plasma membrane activity ("wobbling") of the basal cells, but unlike hypotonic solution, it did not induce wound-polarized lamellipodia or directional cell migration after isotonic injury (Video 6). This suggests that the mechanisms of rapid epithelial defense and repair diverge downstream of the shared osmotic trigger.

Many cells respond to osmotic swelling with nucleotide secretion (Hoffmann et al., 2009). Nucleoside triphosphates (NTPs), such as ATP, are present in the cytoplasm of all cells at high concentrations ([ATP] $\sim$5 mM; Beis and Newsholme, 1975). Vesicular NTP concentrations can be an order of magnitude higher ([ATP] $\sim$90 mM; Johnson, 1988). NTPs may enter the interstitial space via cell lysis, exocytosis, or nucleotide conducting pores. In mammalian cell culture wound healing models, ATP has been found to mediate cell migration via P2Y2 receptor signaling (Yin et al., 2007; Block and Klarlund, 2008; Boucher et al., 2010). It is unclear if similar mechanisms are operant in vivo.

To test for osmotically induced ATP release, we wounded larvae in isotonic medium supplemented with firefly luciferase and luciferin. This experimental setup generates luminescence when ATP is released from the fish into the bathing medium. Detection of ATP by firefly luciferase is highly specific (Moyer and Henderson, 1983). The membrane-impermeable DNA-specific dye SYTOX Orange, which enters cells upon plasma membrane damage, was added to highlight the wound margin and monitor cell lysis. Over an isotonic incubation period of 10 min (unpublished data), or 20 min after tail fin tip amputation, there was no detectable ATP secretion at the wound margin (Fig. 5 a, left; and Fig. 5 b, kymograph between −20′ and 0′). After overlaying the isotonic mounting agarose with a bolus of hypotonic medium, the time required for tonicity equilibration largely depends on the agarose/medium volume ratio. In this experimental setup, we typically observed the first physiological responses, including wound margin compaction and leukocyte recruitment, at $\sim$10–20 min after hypotonic shifting. Dilution of isotonic bathing medium triggered luminescence flashes at

the wound margin (Fig. 5 a, right, green; and Fig. 5 b, kymograph, $\sim$30′–80′) after a 16 ± 3 min (mean ± SEM) lag period. Notably, control experiments revealed that light emission by luciferase itself is quenched $\sim$2× by isotonic solutions (Fig. S3 a). However, given the typical amplitudes of ATP flashes and the detection sensitivity of our assay, the complete absence of flashing activity during isotonic incubation cannot be explained by luminescence quenching (Fig. S3 b). Consistent with previous findings (Enyedi et al., 2013), hypotonicity did not considerably increase cell lysis (SYTOX Orange staining; red in Fig. 5 a; and quantified in Fig. 5 c and Video 7). We conclude that a drop in interstitial osmotic pressure triggers nonlytic ATP secretion from wounded tail fins.

Extracellular nucleotide hydrolysis regulates the range and duration of epithelial cell recruitment

Owing to rapid extracellular hydrolysis by nucleotidases (e.g., ecto-NTP diphosphohydrolases [ENTPDs]; Zimmermann et al., 2012), extracellular ATP half-life in intact tissues is extremely short (ranging from seconds to milliseconds), starkly contrasting its approximately minute-scale half-life in cell culture (Orriss et al., 2009, 2013). Thus, increasing ATP half-life through ENTPD inhibition presents a sensitive method to probe the physiological role of NTPs as regulators of the wound response in vivo. We identified *entpd3* as the most abundant *entpd* isoform in the basal epidermis by FACS sorting of basal epidermal cells expressing GFP under the *ΔNp63* promoter (Reischauer et al., 2009), and semiquantitative RT-PCR (Fig. S4, a and b). Analogously, mammalian ENTPD3 is expressed in wet epithelia of the digestive tract (e.g., stratified linings of the esophagus; Lavoie et al., 2011). For genetic interference, we designed a translation-blocking morpholino (*entpd3* MO1) and a splice-blocking morpholino (*entpd3* MO2) against zebrafish *entpd3*. *entpd3* MO1 produced no major morphological defects besides cardiac edema (Fig. S4 c). *Entpd3* MO2 produced a truncated *entpd3* mRNA, which exhibited no gross morphological defects (Fig. S4 c). Both morpholinos had no obvious morphological effects on the tail fin epithelium (Fig. S4 c). To chemically interfere with extracellular nucleotide hydrolysis, we used adenosine 5′-[γ-thio] triphosphate (ATPγS; a slow-hydrolyzing ATP analogue that, owing to its structural analogy to ATP, is expected to competitively inhibit all ATP hydrolyzing enzymes in the extracellular space) and the ENTPD subgroup-selective antagonist polyoxometalate (POM)/compound 7 (Müller et al., 2006).

Entpd3 knockdown by both morpholinos consistently increased the range and duration of wound-induced epithelial sheet motion (Fig. 6, a and b; and Fig. S4 d). This motion phenotype could be partially rescued by co-injecting *entpd3* MO1 with morpholino-resistant *entpd3* mRNA (Fig. 6 b, blue vs. red curve), arguing against an off-target effect. Enhanced tissue motion was not observed upon injection of an *entpd3* MO1 five-nucleotide mismatch control morpholino (MO1 5 mm), excluding nonspecific morpholino effects (Fig. 6 c). Wound-induced epithelial sheet motion was blunted by the addition of apyrase to the fish bathing medium (Fig. 6 d). The genetic
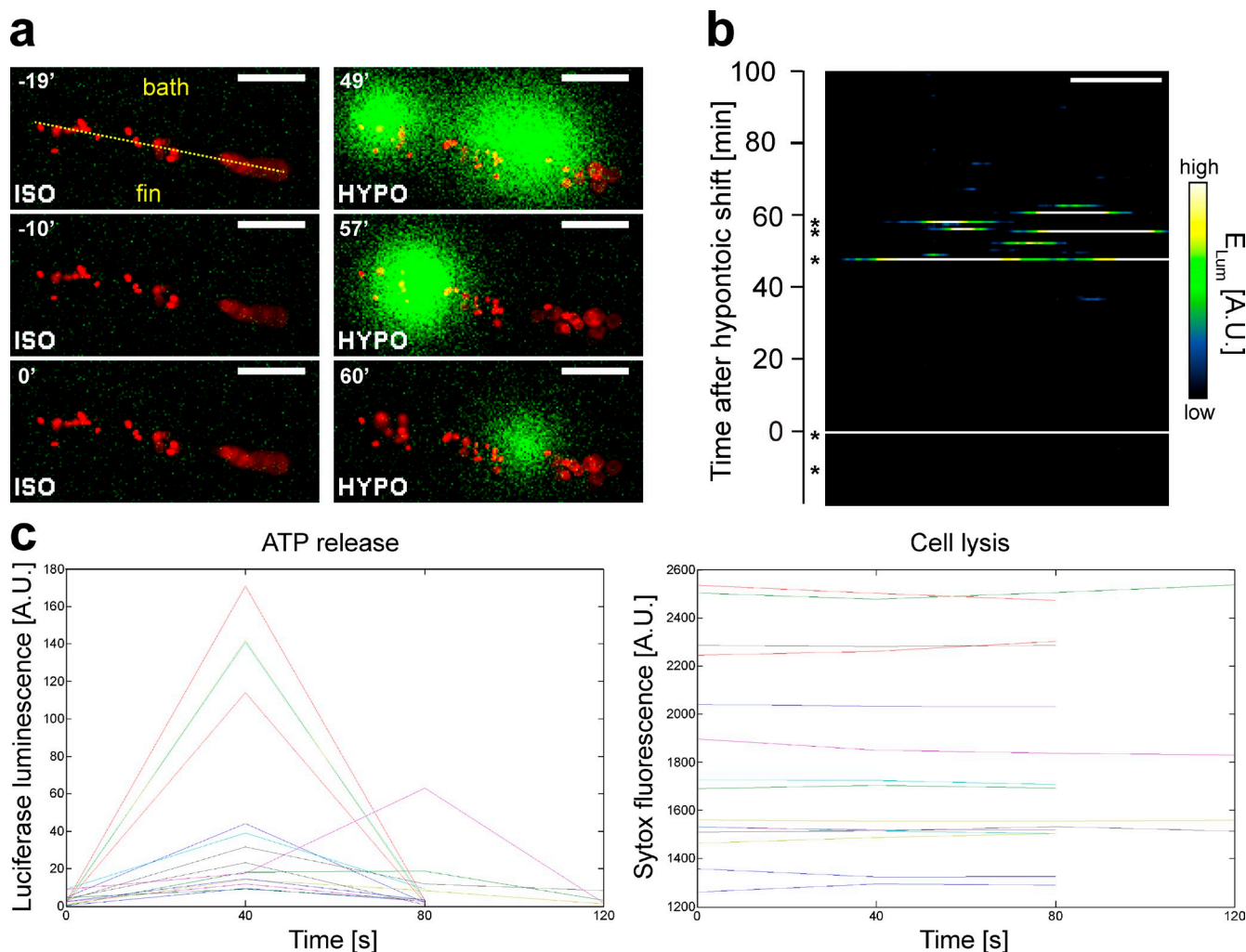
Figure 5. **A drop in interstitial osmotic pressure triggers ATP release in wounded tail fins.** (a) Representative fluorescence/luminescence images from a zebrafish larva at the indicated times after tail fin amputation in isotonic mounting agarose. After 20 min of isotonic incubation (left), the fish was overlaid with a bolus of hypotonic bathing solution (right). Red, SYTOX orange. Green, luminescence. Orientation of the tissue relative to the wound margin (yellow broken line) is indicated. Bars, 100 µm. (b) Representative kymograph ($n = 6$ for 20 min isotonic preincubation, $n = 4$ for 10 min isotonic preincubation) of luminescence emissions acquired by line scans of the wound margin (yellow broken line in Fig. 5 a). Asterisks mark the representative time points (shown in a) on the kymograph. White/yellow, high luminescence emission. Blue/green, low luminescence emission. Bar, 100 µm. (c) Representative intensity plots of the time-lapse data shown in panel a displaying either luciferase luminescence (left) or SYTOX orange fluorescence (right); plots correspond to intensity measurements taken within a 100-µm-diameter region of interest around the center of each ATP luminescent flash. Measurements start one frame before, and end 1–2 frames after each luminescence peak (40 s per frame). Color-coded traces correspond to matching measurements of respective luminescence and fluorescence. The intensity measurements were performed on one representative sample from the dataset depicted in a.

results were corroborated by the pharmacologic inhibition data. As expected, ATPγS produced a dramatic increase in wound-induced tissue motion, which is consistent with its ability to compete with extracellular ATP hydrolysis in general (i.e., not only with ENTPD-mediated hydrolysis; Fig. 6, e and f). POM produced a similar, though less pronounced, motion phenotype (i.e., prolonged epithelial migration), which is consistent with its more restricted target selectivity (as compared with ATPγS; Fig. 6 g). As expected, POM and ATPγS (Video 8) promoted lamellipodia formation in cells far from the wound margin in hypotonicity. The migratory response that ATPγS elicited in hypotonic solution was often so massive that it globally distorted the tissue structure, producing sample drifts (which were corrected by computational image registration when possible;

Video 8). Importantly, these dramatic epithelial migration phenotypes were not induced by pharmacological inhibitor treatment per se, but only in conjunction with hypotonicity (Fig. 6, f and g). This is consistent with the idea that hypotonic, but not isotonic, injury leads to the release of a pro-migratory signal that is NTPase sensitive. Interestingly, although inhibition of interstitial NTP breakdown generally increased sheet motion, aberrant motion typically did not lead to faster wound closure. Rather, it tended to antagonize the normal spatially and highly coordinated, concentric closure movements. Not unexpectedly, efficient wound closure likely requires both epithelial sheet motility (in this case driven by lamellipodia formation in the basal epithelial layer) and proper spatial coordination of collective cell migration.
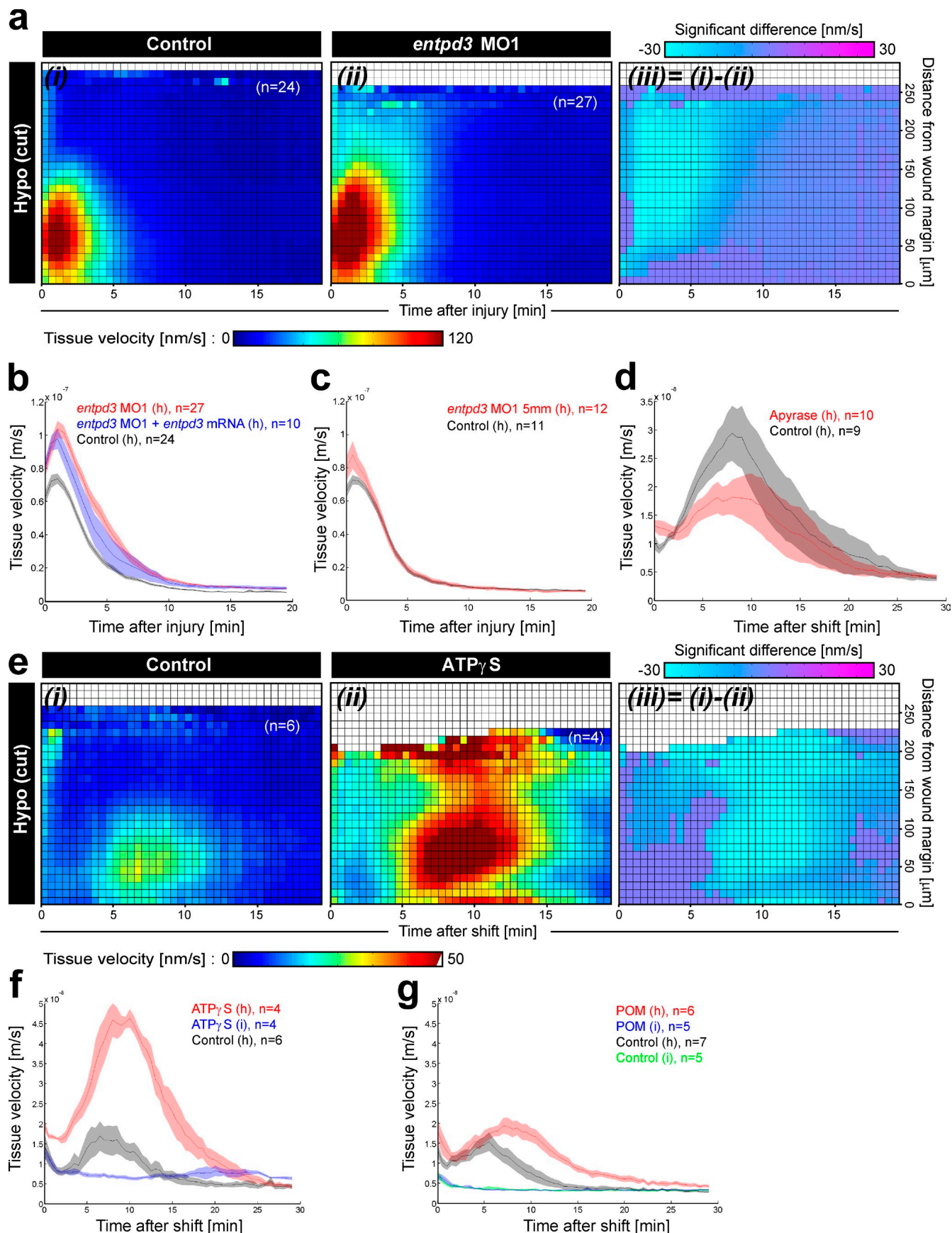
Figure 6. **Epithelial movements in response to hypotonic injury are regulated by extracellular NTP hydrolysis.** (a, i and ii) Spatial PIV analysis of the indicated number of *Tg(krt4:AKT-PH-GFP)* larvae subjected to UV laser cut injury in hypotonic medium, with or without translation morpholino-mediated

ATP reconstitutes cell migration in the absence of environmental hypotonicity

To mimic transient ATP concentration peaks that cells in a tissue may experience immediately after nonlytic ATP release by exocytosis or channel conductance, we supplemented isotonic bathing solution with cytoplasmic levels of ATP. This strongly stimulated basal cell migration in isotonicity as indicated by induction of lamellipodial protrusions toward the wound, and velocimetry analysis (Fig. 7, a and b; and Video 9). As expected, the response was abrogated by pre-incubating the ATP solution with apyrase before adding it to the larvae (Video 9). This excludes the possibility that contamination of the ATP solution stimulated motility. UTP, like ATP, stimulated basal cell motility (Fig. S5 a). The finding that physiologically relevant extracellular concentrations of ATP or UTP can promote epithelial cell motility after isotonic wounding is consistent with secreted NTPs providing a wound-relevant chemokinetic signal. This also shows that isotonicity blocks a migratory stimulus for epithelial cells, but not their general ability to migrate. Although UTP potently induced basal cell migration, our data do not determine whether it is actually released, as luciferase is highly specific for ATP, but not UTP (Moyer and Henderson, 1983). UTP and ATP can be rapidly interconverted by ecto-nucleoside diphosphokinases in the extracellular space of tissues (Lazarowski et al., 1997).

The NTP sensing mechanism underlying basal epithelial responses in our system remains unclear. Our current data indicate that it differs from previously reported purinergic mechanisms involved in wound repair in vitro. Suramin, a nonspecific P2 receptor inhibitor commonly used to block P2Y2, had little effect on rapid wound closure, even at high concentrations (Fig. S5 b). The agonist profile of basal epithelial migration in our system does not match known P2 receptor profiles (Table S1 and Videos 9 and 10). Furthermore, tail fin wound closure occurs much faster than P2Y2-dependent monolayer healing in cell culture. Phylogenetic variations of P2Y specificity or formation of receptor heterodimers may account for this noncanonical behavior. Alternatively, unknown nucleotide receptors may exist. The unexpected discovery of novel ATP receptors in plants, which do not bear sequence similarity to traditional P2 receptors (Choi et al., 2014), underlines this possibility. Our ongoing efforts are directed toward identifying the molecular specifics of NTP release and sensing in our model.

Discussion

Purse string contraction of the wound margin and basal cell sheet migration are the two most plausible wound closure mechanisms that are relevant to our model. Alternative wound closure phenomena, such as cell or matrix contraction, are unlikely to contribute because of the rapid nature of the wound closure and full thickness loss of cells and matrix in the wound region. Although we observe fingerlike protrusions at the wound margin, the almost perfectly circular shape of the wound during closure and its remarkably rapid kinetics argue against a slower zippering mechanism.

Pharmacological Rho kinase inhibition reveals that our laser puncture wounds largely close in the absence of a purse string, albeit not as well coordinated as in the control samples and with a higher incidence of "jagged" and deformed wound margins. Hence, the contractile actin cable cannot be the major mediator of osmotically stimulated wound closure. Likewise, our data do not bear evidence that purse string formation or contraction depends on osmotic cues. The actin cable still forms and rounds up at the wound margin after isotonic injury (Fig. 1 b), which indicates intrinsically stimulated local force generation at the margin even in the absence of the hypotonic trigger. In contrast, we find that lamellipodia formation, migration of basal epithelial cells, and epithelial sheet movement are strongly inhibited by environmental isotonicity. Collectively, this argues that rapid wound closure is mainly mediated by hypotonically induced basal cell migration in our model, although basal cell–specific inhibition of lamellipodial migration would be required to test the contribution of the basal cells to wound closure more directly. To our knowledge, this is the first study delineating different wound closure mechanisms in a complex, bilayered epidermis. Intriguingly, contractile- and actin polymerization–mediated modes of wound closure appear to be spatially separated between different tissue layers, and show different environmental sensitivity. In motile cells, Rho-driven myosin contractility and Rac-driven actin polymerization are believed to antagonize each other, requiring spatial front-back separation to allow coordinated movements. Spatial separation of these mechanisms within multicellular structures may facilitate coordinated tissue movements during wound closure.

Consistent with preceding cell culture studies (Praetorius and Leipziger, 2009), we find that environmental hypotonicity induces nucleotide release at the wound site, most likely through

knockdown of *entpd3* mRNA (*entpd3* MO1; ∼19 ng). (b) Global PIV analysis of the datasets in panel a additionally including morpholino-rescue data (blue curve). (c) Global PIV analysis of MO1 five-nucleotide mismatched control morpholino (*entpd3* MO1 5 mm; ∼19 ng). (d) Global PIV analysis of *Tg(krt4: AKT-PH-GFP)* larvae subjected to mechanical tail fin tip amputation in isotonic solution ± potato apyrase (50 U/ml). After a 10-min preincubation in isotonic mounting agarose with or without apyrase, fish were overlaid with a bolus of hypotonic solution (to initiate the wound response) with or without apyrase. Note that velocimetry analysis does not include the isotonic preincubation period (i.e., t = 0′ in plot is 10′ after injury). (e, i and ii) Spatial PIV analysis of the indicated number of *Tg(krt4:AKT-PH-GFP)* and *Tg(krt4:AKT-PH-mKate2)* larvae subjected to UV laser cut injury in hypotonic medium, with or without ATPγS to globally inhibit extracellular NTP hydrolysis. After a 10-min preincubation in isotonic mounting agarose ± 5 mM ATPγS (in the interface drop), fish were overlaid with a bolus of hypotonic solution (to initiate the wound response) ± 5 mM ATPγS. As in d, the velocimetry analysis does not include the isotonic preincubation period. (e, iii) Differential plot derived by subtraction of the indicated velocimetry plots, and *t* test filtering of statistical significant differences between experimental groups. Statistically significant velocity differences are color-coded (turquoise to pink). Pink, positive values. Turquoise, negative values. (f) Global PIV analysis of the above datasets including data representing the effect of ATPγS after isotonic injury (blue curve). (g) Global PIV analysis of *Tg(krt4:AKT-PH-GFP)* larvae subjected to UV laser cut injury in isotonic/hypotonic solution ± POM (ENTPD inhibitor, 100 µM). After a 10-min preincubation period in isotonic mounting agarose ± POM, fish were overlaid with a bolus of hypotonic (to initiate the wound response) or isotonic solution ± POM. Note that velocimetry analysis does not include the isotonic preincubation period (i.e., t = 0′ in the plot is 10′ after injury). See also Video 8.

nonlytic cell swelling. Notably, our luciferase/luciferin bathing technique is limited by diffusion of luciferase (dimer mol wt ∼120 kD) and luciferin from the bathing medium through the open wound into the tissue. While highlighting the fraction of ATP directly released into the bathing solution, our current measurements may underestimate the actual ATP release pattern due to the limited availability of luminescence-generating enzyme/substrate inside the tissue. Future studies, e.g., with transgenically expressed, membrane-bound luciferase, may allow measurement of ATP release deeper within the tissue.

The mechanisms of swelling-induced ATP release in cells are incompletely understood even in simplified cell culture systems. Besides osmotic cell lysis, hemi-channel conduction (e.g., via connexins or pannexins) and vesicular NTP release appear to be important. Our current results do not argue for cell lysis being a mediator of wound-induced ATP release. Whether any of the other known nonlytic mechanisms accounts for wound-induced ATP release in zebrafish tail fins remains to be investigated.

If extracellular NTPs are endogenous mediators of basal cell migration in our model, epithelial sheet motion should be inhibited by increasing extracellular NTP breakdown. Likewise, decreasing extracellular NTP hydrolysis should enhance epithelial sheet motility. Collectively, our genetic and pharmacologic perturbations of extracellular nucleotide metabolism, including morpholino-mediated knockdown of the most abundant ENT-PDase of basal epithelial cells, (*entpd3*), confirm these predictions. ATP bathing triggers basal cell migration, but does not fully reconstitute hypotonic wound closure. A possible explanation for this could be that ATP bath application is unlikely to recapitulate the endogenous, spatiotemporal ATP release pattern, which may be crucial, e.g., for proper spatial coordination of collective movements. In addition, ubiquitous exposure of larvae to high ATP concentrations on the outside, apical surface of suprabasal cells may adversely affect the behavior of the suprabasal layer during closure. Finally, our data do not exclude that there are other unknown, hypotonically triggered processes, in addition to NTP release, that contribute to rapid wound closure.

In this study, we have identified an osmotic signaling circuit that initiates extracellular ATP release in response to a drop of interstitial osmotic pressure. This autoregulatory mechanism adjusts wound responses to wound size by coupling basal cell migration to environmental exposure (Fig. 7 c). Intriguingly, the same osmotic cue that mediates rapid wound detection by leukocytes via eicosanoids (Enyedi et al., 2013) also mediates rapid wound closure by nucleotides. Only very few reports have addressed potential environmental contributions to tissue healing and regeneration, including classic work by Goldfarb and Loeb (Loeb, 1891; Goldfarb, 1907, 1914; Radice, 1980; Fuchigami et al., 2011). To date, wound repair is still predominantly viewed as an organism-intrinsic process driven by cell damage, lack of contact inhibition, or altered mechanical signaling at tissue edges. Our study advances this concept by illuminating how environmental surveillance regulates rapid epithelial repair through osmotic signaling in vivo. Transepithelial gradients of osmotic pressure, comparable to those that zebrafish experience in freshwater, exist in the human mouth and esophagus. Furthermore, steep transepithelial pH gradients occur in the stomach. It will be interesting to determine whether these chemical gradients mediate environmental surveillance of mammalian wet epithelia.

Materials and methods

General zebrafish procedures
Adult AB wild-type (wt), casper (White et al., 2008), and transgenic zebrafish strains were maintained according to institutional animal guidelines, and as described previously (Nusslein-Volhard and Dahm, 2002). Zebrafish larvae were raised in E3 medium (5 mM NaCl, 0.17 mM KCl, 0.33 mM CaCl$_2$, and 0.33 mM MgSO$_4$). For wounding assays, 2.5–3 days postfertilization (dpf) larvae were anesthetized using 0.2 mg/ml tricaine (Sigma-Aldrich) in E3 for at least 20 min before and during laser wounding and imaging. To suppress skin pigmentation, larvae were maintained in E3 medium supplemented with 0.2 mM *N*-phenylthiourea (PTU; Sigma-Aldrich) from 1 dpf until the start of the experiment.

Reagents
The following nucleotides, nucleotide analogues, or metabolites were used at a final concentration of 5 mM in isotonic E3 medium: adenosine 5′-triphosphate disodium salt hydrate (ATP; A26209; Sigma-Aldrich), adenosine 5′-[γ-thio] triphosphate tetralithium salt (ATPγS; 4080; Tocris Bioscience), 2′(3′)-*O*-[4-Benzoylbenzoyl]-adenosine 5′-triphosphate triethylammonium salt (Bz-ATP; B6396; Sigma-Aldrich), adenosine 5′-diphosphate sodium salt (ADP; A2754; Sigma-Aldrich), adenosine 5′-[β-thio]-diphosphate trilithium salt (ADPβS; A8016; Sigma-Aldrich), adenosine 5′-monophosphate sodium salt (AMP; A1752; Sigma-Aldrich), adenosine (A9251; Sigma-Aldrich), uridine 5′-triphosphate trisodium salt hydrate (UTP; U6625; Sigma-Aldrich), uridine 5′-[γ-thio]-triphosphate trisodium salt (UTPγS; 3279; Tocris Bioscience), uridine 5′-diphosphate disodium salt hydrate (UDP; 94330; Sigma-Aldrich), 3-[2-Oxo-2-phenylethyl]-uridine-5′-diphosphate disodium salt (3-phenacyl UDP; PSB 0474; Santa Cruz Biotechnology, Inc.), uridine 5′-diphosphoglucose disodium salt hydrate (UDP-glucose; U4625; Sigma-Aldrich), uridine 5′-monophosphate (UMP; U1752; Sigma-Aldrich), and uridine (U3750; Sigma-Aldrich). Arachidonic acid (A9673; Sigma-Aldrich) was used at a final concentration of 10 µM in isotonic E3 medium. The following inhibitor compounds were used: cell-permeable Cytochalasin D (100 µM, 1233; Tocris Bioscience) and Y-27632 (100 µM, 10005583; Cayman) were dissolved DMSO (D8418; Sigma-Aldrich) and diluted in the indicated E3 medium. Cell-impermeable POM (K$_6$H$_2$[TiW$_{11}$CoO$_{40}$]; 100 µM; Müller et al., 2006), apyrase (50 U/ml; A6410; Sigma-Aldrich), ATPγS (5 mM; 4080; Tocris Bioscience), or Suramin (1 mM; S2671; Sigma-Aldrich) were dissolved in the indicated E3 medium. The following reagents were used for luminescence imaging: firefly luciferase (L9506; Sigma-Aldrich) and sodium luciferin (L6882; Sigma-Aldrich), and SYTOX Orange (Life Technologies). Hydrogen peroxide solution (H$_2$O$_2$; 216763; Sigma-Aldrich) was diluted to 1 mM in E3 medium for the barrier reconstitution assay.

Plasmid construction and in vitro transcription
To observe cell/tissue dynamics and morphology, the PH domain of human AKT1 (amino acids 1–147) fused with GFP was used (18836; Addgene; Kwon et al., 2007), or the AKT1 PH-domain was fused in-frame with the far-red fluorescent protein mKate2 (Evrogen). The AKT-PH-GFP was subcloned from pcDNA-AKT-PH-GFP (18836; Addgene) into pCS2+ (Sp6 promoter) with EcoRI–XbaI. The AKT-PH cassette was PCR cloned from pcDNA-AKT-PH-GFP-GFP into pCS2+ with ClaI–EcoRI upstream of mKate2. To observe myosin II localization during wound closure, human myosin regulatory light chain 1 (mrlc1) was PCR amplified from pEGFP-mrlc1 (35680; Addgene; Beach et al., 2011) and cloned into the promoterless middle entry vector pME (tol2kit) with XhoI–HindIII, in frame with mKate2. mrlc1-mKate2 was PCR amplified from pME and cloned into pCS2+ with XhoI–XbaI. pCS2+GFP-Utrophin calponin homology domain (GFP-UtrCH) was created as described previously (26737; Addgene; Burkel et al., 2007). In brief, UtrCH (amino acids 1–261) was cloned into the BspE1–XhoI sites of the pCS2-EGFP plasmid (sp6 promoter). *entpd3* MO1 insensitive was cloned using the following primers (mutations in lower case): Entpd3_mut_fwd, 5′-AAGCTTATGATtAAcAAaGAaTCaCAaTCTTCAGACCACCTTAC-3′; and Entpd3_rev, 5′-GCTTCTAGAACCTCAATAACAGTAGCGCAC-3′ into the HindIII and XbaI sites of pME, then subcloned into ClaI–XbaI sites of pCS2+. In vitro transcription of mRNA from pCS2+ plasmids was performed using the mMessage mMachine Sp6 kit (Life Technologies), following plasmid
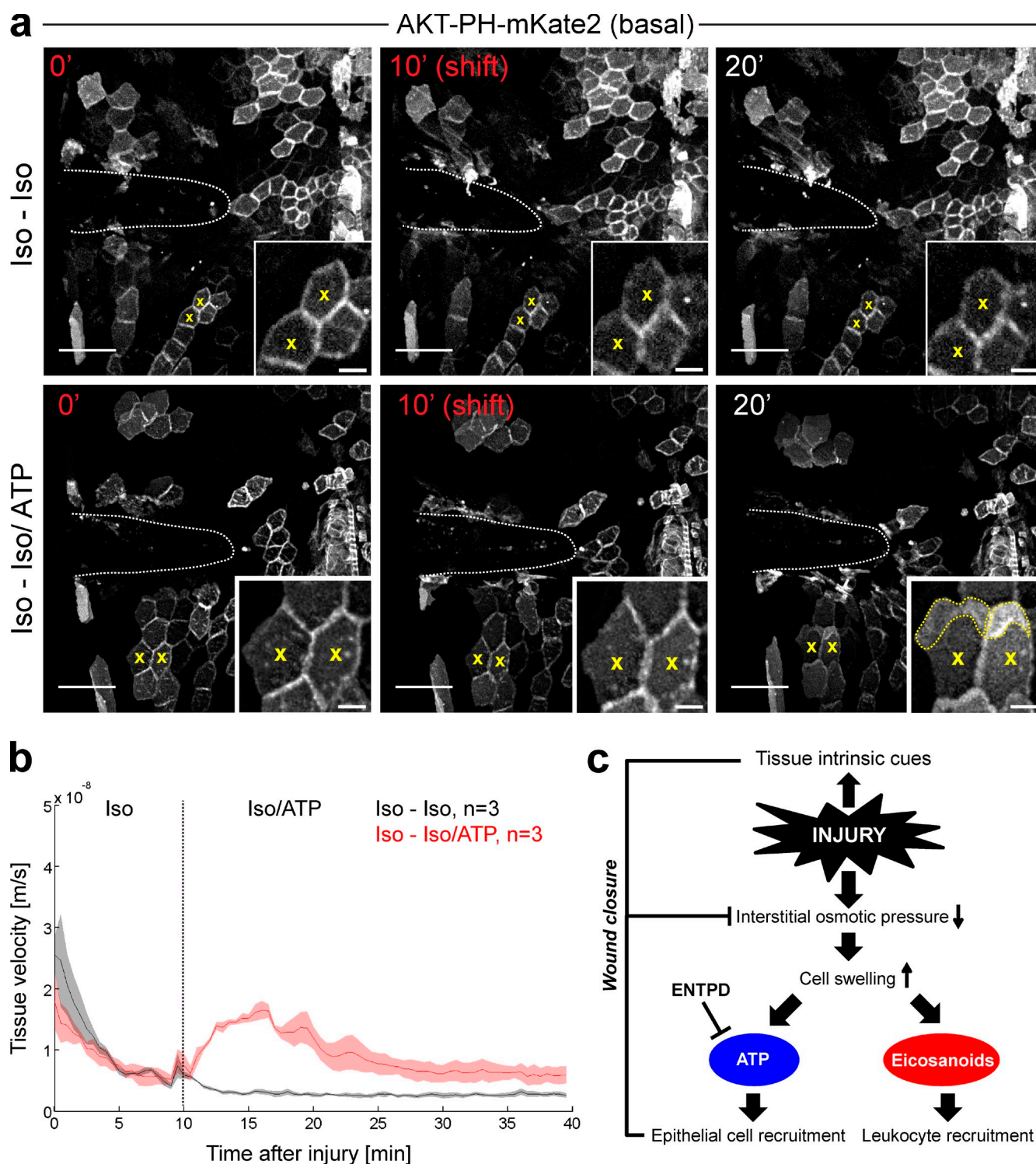
Figure 7. **ATP reconstitutes basal cell migration and epithelial sheet movement in the absence of a transepithelial osmotic gradient.** (a) Representative time-lapse images of zebrafish larvae exhibiting mosaic plasma membrane AKT-PH-mKate2 labeling of predominately basal cells (4–8-cell-stage mRNA injection). Larvae were subjected to UV-laser-cut wounding in isotonic mounting agarose. After 10 min of isotonic preincubation (red time indices), a bolus of isotonic solution ± 5 mM ATP was added to the imaging dish. Yellow x, representative morphological response after addition of isotonic solution ± 5 mM ATP. Note that formation of AKT-PH-mKate2–rich membrane protrusions (yellow broken line) after iso-iso/ATP, but not iso-iso shifting. The same representative iso-iso control and data set were used in Fig. S5 a. See also Video 9. Bars: (main panels) 50 μm; (inset) 10 μm. (b) Global PIV analysis of the indicated number of larvae exhibiting ubiquitous plasma membrane labeling (one-cell stage AKT-PH-mKate2 mRNA yolk injection). Larvae were subjected to UV-laser-cut wounding in isotonic mounting agarose. After 10 min of isotonic incubation, a bolus of isotonic medium ± 5 mM ATP was added to the sample. (c) Proposed circuitry scheme of tissue intrinsic and environmentally triggered branches of the wound response in zebrafish tail fins. Tissue-intrinsic mechanisms include purse-string contraction (not depicted). Environmentally dependent osmotic surveillance through secretion of nucleotides (epithelial cells) and eicosanoids (leukocytes) is depicted.

linearization with either NotI or Asp718. Akt-PH-GFP was subcloned from pcDNA-AKT-PH-GFP (18836; Addgene) into EcoRI–XbaI of pME, and Akt-PH-mKate2 was subcloned from pCS2+Akt-PH-mKate2 into ClaI–XbaI of pME. GFP-UtrCH was PCR amplified from pCS2+GFP-UtrCH and ClaI–BamH1 cloned into pME. To construct plasmids for transient mosaic expression or the generation of stable transgenic zebrafish, the tol2kit system was used (Kwan et al., 2007); pME-AKT-PH-GFP, pME-AKT-PH-mKate2, or pME-GFP-UtrCH were combined with plasmids containing either the *actb2* (Higashijima et al., 1997) or keratin4 (*krt4*; previously *krt8*; Gong et al., 2002) promoters and an SV40 poly-A sequence into the pDestTol2CG2 backbone (Kwan et al., 2007) using gateway cloning (Invitrogen). *ΔNp63: Gal4,UAS:GFP* was generated as described previously (Reischauer et al., 2009). In brief, the *ΔNp63* promoter was cloned (blunt-ended HhaI) into a miniTol2 plasmid upstream of the Gal4 transcription factor sequence and an upstream activation sequence (UAS) driving the expression of GFP.

Generation of transgenic lines

To create *Tg(krt4:AKT-PH-GFP)*, *Tg(krt4:AKT-PH-mKate2)*, or *Tg(ΔNp63: Gal4,UAS:GFP)* transgenic zebrafish, 25 pg of each construct was co-injected with 25 pg transposase mRNA into the cytosol of one-cell stage casper embryos (White et al., 2008). Potential transgenic larvae were selected based on heart-specific expression of EGFP driven by the cardiac myosin light chain (cmlc) promoter, or by mosaic GFP expression from the *ΔNp63:Gal4,UAS:GFP* construct. Candidate transgenic larvae were grown to sexually maturity, and then crossed to wt fish. Founder animals with germline integration of the transgene were identified by heart fluorescence (Tol2 transgenic constructs) or basal cell–specific GFP expression (miniTol2 *ΔNp63:Gal4,UAS:GFP* construct). Founders were crossed to caspers, or subsequent F1 transgenic siblings were crossed together to obtain the 2.5–3-dpf transgenic larvae used in the wounding experiments.

Epidermal layer-specific cell labeling

One-cell stage yolk injections of mRNA (0.5–1 ng) encoding GFP-UtrCH, MRLC-mKate, or AKT-PH-mKate2 were used to visualize F-actin, Myosin II, or plasma membrane (PIP3), respectively, in both epidermal layers (basal and suprabasal). To observe cells in the suprabasal epidermal layer exclusively, cDNA-encoding AKT-PH-GFP, AKT-PH-mKate2, or GFP-UtrCH was expressed under the control of the *krt4* promoter (see "Plasmid construction and in vitro transcription"). Labeling of plasma membranes in the basal cell layer was achieved by mosaic expression of AKT-PH-GFP or AKT-PH-mKate2. To this end, mRNA (0.5–1 ng) was injected into the yolk of 4–8-cell-stage embryos. 2.5–3-dpf larvae with strong, mosaic expression in the tail fin were selected for experiments. Basal cells are distinguishable from superficial cells by morphological characteristics, including cell shape and the degree of enrichment of membrane markers such as PH-mKate2 or PH-GFP (Fig. 2). This basal cell labeling strategy was validated by injecting AKT-PH-mKate2 mRNA into the yolk of 4–8-cell *Tg(krt4:AKT-PH-GFP)* embryos, which demonstrated that the majority of AKT-PH-mKate2 was expressed in epithelial cells underlying the GFP-positive suprabasal layer (Fig. 2). *ΔNp63:Gal4,UAS:GFP* plasmid injection (25 pg) into the cytosol of one-cell-stage casper or AB embryos, or stable transgenic expression was also used to specifically label basal epidermal cells. *actb2:Akt-PH-GFP* plasmid (25 pg) injection into the cytosol of one cell stage casper or AB embryos, followed by preselection, permitted mosaic basal cell labeling for the cell tracking experiment.

Confocal imaging and laser wounding

For epithelial wounding experiments, anaesthetized 3-dpf larvae were immobilized on a plastic Petri dish by embedding in ∼200 µl 1% low-melting-point agarose dissolved in either standard hypotonic E3 fish medium, Iso$_{NaCl}$ (E3 medium supplemented with 135 mM NaCl$_2$), or Iso$_{Sucrose}$ (E3 supplemented with 270 mM sucrose), and for pharmacological inhibition experiments, supplemented with the indicated concentrations of inhibitor compounds. The same respective medium was used for immersion. Cut (tail fin edge) or puncture (round internal) wounds were induced with several quick successive laser pulses (3–4 passes) using a microscope-mounted 435-nm ultraviolet MicroPoint laser (Andor Technology). Laser cutting generated triangular wounds on the tip of the tail fin. Puncturing was performed in a region equidistant between the notochord and the tail fin edge. In both contexts, tissue was ablated to a similar degree from both sides of the fin fold. Shifting experiments (Iso to Hypo, or Iso to Iso) were performed by embedding larvae in a 10–200-µl volume of 1% low-melting agarose supplemented with the indicated osmolytes, and/or pharmacological compounds. A small drop of the respective isotonic E3 medium was applied to the solidified agarose to create an interface with the objective lens. After isotonic preincubation for the indicated times, a bolus of Hypo-E3 (or Iso-E3) shifting medium supplemented with the indicated concentration of compounds was added to the imaging dish (at least a 10× agarose equivalent volume). Note: unless otherwise indicated, the "Isotonic" or "Iso" referred to in the manuscript is Isotonic$_{NaCl}$ (E3 medium supplemented with 135 mM NaCl$_2$). All experiments were performed on a microscope (Eclipse FN1; Nikon) with a 25× Apochromat LWD NA 1.1 water immersion objective lens (Nikon). EGFP and mKate2 fluorescence was excited using 488 nm and 561 nm diode laser lines (Revolution XD; Andor), respectively. mKate2 emission was acquired using a 620/30 band-pass filter. EGFP emission was acquired using a 535/20 band-pass filter (Chroma Technology Corp.). Images were acquired with an EM CCD camera (iXon3 897; Andor) and NIS-Elements software (Nikon). Experiments were performed at room temperature (∼26°C).

Epithelial cell tracking and morphometric analyses

Spinning disk confocal time-lapse stacks of wounded tail fins mosaically expressing PH-AKT-GFP in the basal cells were z-projected (maximum-intensity projection), and brightness and contrast enhanced in Fiji (an ImageJ package). The center of mass of basal cells in the imaging field was tracked using the MTrackJ plugin of Fiji. Linear cell displacement (D) was approximated as $D = D_{CW}(0') - D_{CW}(19')$, with D_{CW} being the Euclidian distance between center of mass of a cell and the center of mass of the wound area either 0 min or 19 min after injury. We found this type of measurement to be more robust with regards to occasional sample drifts, as displacement is expressed in relation to wound center of mass. This calculation assumes that epithelial cells migrate roughly linearly on the shortest path to the wound, which is a decent approximation for most epithelial cells. Mean displacement distance of cells was plotted as a function of binned (12 µm), initial wound distance of these cells ($D_{CW}(0')$). Negative values in the binned displacement data are attributed to sample drift. The wound area was assessed in 2.5–3-dpf *Tg(krt4:AKT-PH-GFP)*, or in GFP-UtrCH mRNA–injected larvae. ∼5,000 µm² puncture wounds were generated by 3–4 rapid successive UV laser pulses, which produced wounds on both sides of the epithelial fold (i.e., two wounds). The area of the wound proximal to the objective lens was measured by using the polygon selection tool in Fiji to outline the wound margin. The *Tg(krt4:AKT-PH-GFP)* dataset, which was part of the wound area quantification (Fig. 1 b), was used for velocimetry analysis in Fig. 4.

Velocimetry analysis

Spinning disk confocal time-lapse stacks of wounded tail fins expressing PH-AKT-GFP (or PH-AKT-mKate2) in the suprabasal epithelial layer (*Tg(krt4: AKT-PH-GFP)* or *Tg(krt4:AKT-PH-mKate2)*) were z-projected (maximum-intensity projection), convoluted (3 × 3 × 1 matrix, Fiji "Convolve" command), background subtracted, and contrast enhanced in Fiji. Tissue velocities were measured by calculating particle motion between subsequent images of the time lapse using MATLAB (R2010b; MathWorks) with the open source PIV analysis software PIVlab v1.32 (developed by W. Thielicke and E.J. Stamhuis). In brief, the program split each frame into 63 × 63 interrogation windows for which the respective displacement vectors between subsequent frames were calculated. This yielded a 63 × 63 velocity vector matrix that was masked to eliminate regions of low image intensity. The masked PIVlab-generated velocity vectors were either (1) averaged within the program to generate global velocity (averaging of all velocity vectors magnitudes in the unmasked field of view) as a function of time after injury, or (2) matrices were further analyzed (spatially resolved) with self-written MATLAB functions to express particle velocity magnitude ($|v|$) as function of binned distance (10 µm bins) of the respective PIV-interrogation window from the wound margin (D_{margin}), and time after injury. For puncture wounds, the wound region was computationally determined in each image using an edge detection algorithm. The Euclidian distance (D_c) of the PIV-interrogation window from the center of mass of the detected wound area was determined. For puncture wounds (i.e., roughly round wounds), wound margin distance of each PIV-interrogation window was approximated as $D_{margin} = |D_c - r_w|$, with r_w being the radius of a circle with the same area as the computationally determined wound region. For laser cut wounds, a polygonal region of interest was manually selected from the last frame of the time-lapse stack to outline the wound area. Then, D_{margin} was calculated as minimal distance of the PIV-interrogation window from any of the polygon's ribs. Occasionally, fluorescent cell debris interfered with accurate edge detection. To remove bright spots, time-lapse stacks were post-processed using the freehand selection and flood filling tool (Fiji), and then further analyzed in MATLAB as usual. Tonicity shifting experiments typically caused unspecific bulk movements of the specimens due to liquid addition. To eliminate velocity components caused by unspecific bulk

movements, these time-lapse stacks were registered ("StackReg-> Rigid Body" command; Fiji) before PIVlab analysis.

This normalization enabled averaging of spatiotemporal tissue motion profiles over multiple animals, and comparison between different experimental groups. For statistical comparison, averaged velocity maps of different experiment groups were subtracted as indicated, and the corresponding (i.e., with regards to distance from wound margin, and time after injury) velocity values of different experimental groups were tested for significant differences using an unpaired Student's t test (i.e., $P < 0.05$). All statistical insignificant velocity differences ($P > 0.05$) in the subtraction map were set to zero to highlight only statistically significant differences. Means of global velocity vector magnitudes for time-lapse frames were extracted from PIVlab, averaged in Excel, and plotted using MATLAB. The differences in velocity ranges depicted along the y axis of graphs is due to either different treatment methodologies or the type of wound (amputation, cut, or puncture) required to deliver selected compound into the tissue. For example, wounding regimes requiring isotonic to hypotonic shifting to deliver cell-impermeable compounds exhibit velocity ranges that differ from wounding regimes that deliver cell-permeable compounds where shifting was not used. Amputation wounds to deliver larger molecules (e.g., apyrase) also have different velocity profiles than cut or puncture wounds.

H_2O_2 barrier reconstitution assay

To measure epithelial barrier integrity, Tg(actb2:HyPer) larvae were used to visualize the penetration of exogenous H_2O_2, a molecule with similar physicochemical properties as H_2O, through the wound into the cytosol of the cells in the tail fin. The 2.5–3-dpf larvae were subjected to tail fin tip amputation in Iso_{NaCl}-E3 using a needle knife (Fine Science Tools), and were embedded in a small volume of 1% isotonic low-melting agarose ($\sim$300 µl) in a glass-bottom dish (MatTek Corporation) 1 h later. This waiting period was required for the endogenous, wound-induced H_2O_2 signal to diminish, allowing the consecutive measurement to assess the effect of exogenously added H_2O_2. At least a 10× agarose volume equivalent of standard-E3 (hypotonic) or Iso_{NaCl}-E3 (3–4 ml) containing 1 mM H_2O_2 was added on top of the agarose pad when the acquisition started. Every minute, HyPer fluorescence was excited using LED light and 438/57 and 475/28 excitation filters (Lumencor). Emission was acquired using a 535/30 emission filter (Chroma Technology Corp.). Images were acquired at room temperature ($\sim$26°C) using NIS-Elements (Nikon) on a microscope (Eclipse Ti; Nikon) equipped with a 20× Plan-Apochromat NA 0.75 air objective lens, an Andor Clara charge-coupled device (CCD) camera, and a motorized stage. Hyper ratio images (E500/E420) were created by dividing median filtered and background subtracted YFP500 and YFP420 images using Fiji, as described previously (Niethammer et al., 2009; Enyedi and Niethammer, 2013). Oxidized tissue surface area was measured using Fiji by thresholding for HyPer ratio values over 0.64.

Luminescence imaging

Zebrafish tail fin cuts were performed on anesthetized 2.5–3-dpf larvae in a glass-bottom dish within a drop ($\sim$150 µl) of isotonic fish water (Iso_{NaCl}-E3) supplemented with firefly luciferase ($\sim$1.7 mg/ml) and D-luciferin (100 µM), MgSO$_4$ (10 mM), and SYTOX Orange ($\sim$7 µM) using a needle knife. For larval mounting, 100 µl of warm 1.5% low-melting agarose in Iso_{NaCl}-E3 was mixed into the drop containing the luminescence mix and the wounded larvae. After agar solidification, the dish was transferred to an inverted microscope (Eclipse Ti; Nikon) equipped with a 20× Plan-Apochromat NA 0.75 air objective lens, an Andor Clara CCD camera, an LED light source (Lumencor), and a motorized stage. During imaging, the dish was covered with an aluminum-foil covered plastic box to minimize environmental light exposure. Luminescence was acquired using a 525/50 emission filter (Chroma Technology Corp.) using 8 × 8 binning and a camera exposure time of 5 s. SYTOX orange fluorescence was excited using LED light and a 549/15 excitation filter (Lumencor), and its emission was acquired using a 632/60 emission filter (Chroma Technology Corp.). After imaging isotonic wound responses for 10 or 20 min, a bolus ($\sim$3 ml) of hypotonic fish water (i.e., standard E3 + Tricaine) containing 10 mM MgSO$_4$, 5 µM SYTOX Orange, and 150 µM sodium luciferin was added to the isotonic agarose drop in order to initiate the hypotonic wound response. Acquired image stacks were background subtracted, and contrast adjusted using the Fiji software (Schindelin et al., 2012). The luminescence kymograph was prepared by applying the Fiji "reslice" command on a line drawn along the wound margin (as visualized by SYTOX Orange staining). For presentation reasons, luminescence and fluorescence channels were color coded, and superimposed. All images were acquired at room temperature ($\sim$26°C) using the NIS-Elements (Nikon) software. To quantify cell lysis in

response to hypotonicity, a circular region of interest (100 µm) was drawn around each individual ATP flash throughout the time-lapse (Fiji), to measure the intensity of luciferase luminescence and the local SYTOX orange fluorescence. The intensity measurements start one frame before, and end 1–2 frames after each luminescence peak (40 s per frame). Color-coded traces correspond to matching measurements of luminescence and fluorescence, respectively.

To test the effect of tonicity on light generation by luciferase, luminescence was measured in 5-µl drops of isotonic (145 mM NaCl) or hypotonic E3 (5 mM NaCl) supplemented with firefly luciferase (0.5 mg/ml), sodium luciferin (150 µM), and MgSO$_4$ (10 mM), and indicated concentrations of ATP (10–100 µM). Luminescence was acquired using the same settings as above, except that a 4× Plan-Apochromat NA 0.2 air objective lens was used. Background of drop images was acquired in a rectangular area outside the drop, and subtracted from the drop image. A rectangular region covering the center of the drop was measured to obtain the mean luminescence using Fiji. Three drops per ATP concentration were measured. Mean luminescence and standard deviation of triplets was plotted as a function ATP concentration, and tonicity (Fig. S3).

Cell sorting and semiquantitative RT-PCR

Basal cell sorting was performed by disaggregating $\sim$200 Tg(ΔN-p63: Gal4, UAS:GFP) transgenic 2.5–3-dpf larvae into a single cell suspension as described previously (Bertrand et al., 2007). In brief, larvae were anesthetized using 0.2 mg/ml tricaine (Sigma-Aldrich) in E3, dissociated using Liberase TM (Roche; 13 U/ml, 15 min at 32°C.), and disrupted mechanically with a pestle. Cell suspensions were passaged through a 40-µm nylon mesh and washed twice in FACS buffer (centrifugation at 250 g for 5 min). Cell sorting of GFP-positive cells was performed on a FACS (Aria III; BD) using 488-nm excitation and 530/30-nm emission wavelengths. mRNA was extracted with oligo (dt)25 Dyna Beads (Invitrogen), followed by cDNA synthesis with RevertAid First Strand cDNA Synthesis kit (Thermo Fisher Scientific), and PCR Phire Hot Start II DNA polymerase (Thermo Fisher Scientific) using the following gene primers (PCR cycle numbers referred to in Fig. S4 b are indicated below):

entpd1 (ENSDARG00000045066). entpd1_fwd: 5′-ATAGTCCTGGAT-GCCGGCTC-3′, entpd1_rev: 5′-GGGGTTTCGCTGTGTCTGTG-3′ (33 PCR cycles).

entpd2a.1 (ENSDARG00000035506). entpd2a.1_fwd: 5′-ACATCAAA-GGGTCACCAGGCTT-3′, and entpd2a.1_rev: 5′-GTAGTCTCATGCCCG-CTGTG-3′ (35 PCR cycles).

entpd2a.2 (ENSDARG00000033953). entpd2a.2_Fwd: 5′-CCATCAC-GTCTCCAGCGGATTT-3′, and entpd2a.2_Rev: 5′-AAGAGACCAGCCGA-CAGAGG-3′ (33 PCR cycles).

entpd2b (ENSDARG00000044795). entpd2b_Fwd: 5′-GGACACGAG-TATTCCCTCTACACG-3′, and entpd2b_Rev: 5′-GCTTGTGTAGCCTCCTC-TAGCTGT-3′ (41 PCR cycles).

entpd3 (ENSDARG00000035309). entpd3_Fwd: 5′-GGCTCTTCCCG-GACTACTGTGTA-3′; entpd3_Rev: 5′-CTGTCTTAGCCCCATGAGGATG-TAC-3′ (33 PCR cycles).

entpd8 (ENSDART00000011245). entpd8_Fwd: 5′-CTCTTGCAAACC-GGCAGACTTT-3′, entpd8_Rev: 5′-ATCCCTGTGAGTATTCTGGCTCCT-3′ (35 PCR cycles).

tp63 (ENSDARG00000044356). tp63_Fwd: 5′-AGCCAAATCTG-CAACCTGGACG-3′, tp63_Rev: 5′-AGGTGACTGGGTGGGGCTAT-3′ (33 cycles).

actb1 (ENSDART00000054987). actin_Fwd: 5′-CCAGACATCAGGG-AGTGATG-3′, actin_Rev: 5′-AGGAAGGAAGGCTGGAAGAG-3′ (32 PCR cycles).

Pharmacological inhibitor treatments and morpholino injections

Cell-permeable pharmacological inhibitors were applied to 2.5–3-dpf zebrafish by preincubation for 60 min in standard E3 or isotonic E3$_{NaCl}$ medium supplemented with the following compounds: Cytochalasin D (100 µM) or Y-27632 (100 µM). For UV laser wounding, larvae were mounted in 1% low-melting-point agarose (Hypo-E3 or Iso_{NaCl}-E3) and overlaid with the respective medium containing the indicated concentration of osmolytes and inhibitors. For inhibition experiments with POM (100 µM), ATPγS (5 mM), or Suramin (1 mM), larvae were mounted, laser-wounded in 1% Iso_{NaCl} E3 agarose supplemented with each compound, and incubated (10 min) with a drop of Iso_{NaCl}-E3 placed at the interface between the dipping objective lens and mounted sample (containing the respective compound). The preincubation period was required for sufficient infusion of the water-soluble compound through the open wound (i.e., kept open with isotonic E3).

A 10× bolus of standard E3 or Iso$_{NaCl}$ E3 medium supplemented with each respective compound was then added to the imaging dish. Apyrase (50 U/ml) inhibition was performed using the identical shifting regimen described for POM, Suramin, or ATPγS, with the exception that tail fin amputation (needle knife; Fine Science Tools) was used to provide a larger opening for apyrase to infuse the tissue (osmolarity readings of the apyrase solutions were identical to the control solutions, ruling out salt contamination in the apyrase stock). For the PIVlab analysis of ATPγS treatment, ATPγS was not administered in the agarose, but added to the interface drop and the shifting medium to prevent excessive drifting of the sample. Imaging was performed for the indicated time using a laser spinning disk confocal microscope (see "Confocal imaging and laser wounding"). Basal cell migration or suprabasal tissue movement were assessed for 20–30 min after shifting. Hydrophobic compounds were dissolved in DMSO, which was applied to samples at a maximal final concentration of 1%.

2.3 nl of 1 mM (~19 ng) translation-blocking morpholino (5′-GACT-GGGACTCCTTATTGATCATGC-3′; MO1; Gene Tools, LLC), translation-blocking five-nucleotide mismatch control morpholino (5′-GAaTGGaACT-CaTTATTaATCATaC-3′; MO1 5 mm; Gene Tools), or splice-blocking morpholino (5′-GGTTGGCTTATACCTTTAACTAGAC-3′, MO2; Gene Tools), targeting the exon3-intron3 of zebrafish *entpd3*, were injected into the yolk of one-cell-stage embryos. For UV laser wounding, larvae were mounting in 1% low-melting-point agarose (Hypo-E3 or Iso$_{NaCl}$-E3) and overlaid with the indicated medium, UV-cut-wounded, and imaged for the indicated time using a laser spinning disk confocal microscope (see "Confocal imaging and laser wounding"). To confirm knockdown efficiency of MO2, mRNA from 2.5–3-dpf old morphant larvae (n = ~20) were extracted using oligo (dt)25 Dyna Beads (Invitrogen). cDNA synthesis was performed with the RevertAid First Strand cDNA Synthesis kit (Thermo Fisher Scientific), and PCR Phire Hot Start II DNA polymerase (Thermo Fisher Scientific), using the following primers: 5′-ATGATCAATAAGGAGTCCCAGTC-3′ and 5′-CTTTT-GGTCTTGATCCCCATCTA-3′. The RT-PCR product was TA-cloned (Agilent Technologies) and sequenced. Morphant *entpd3* mRNA revealed a 31-nt deletion at the 3′ end of exon 3. This deletion is predicted to cause a frame shift resulting in an alternate morphant peptide sequence after aa 90 and a premature stop codon and truncation after aa 97. This is predicted to delete several conserved domains required for surface expression and catalytic function, including four apyrase-conserved regions (ACRs) required for nucleotide binding and hydrolysis (Rosemberg et al., 2010; Zimmermann et al., 2012). Rescue experiments were performed by co-injecting 1 mM (~19 ng) MO1 with 0.1 µg/µl MO1-resistant *entpd3* mRNA (see "Plasmid construction and in vitro transcription") in 2.3 nl.

Isotonic reconstitution experiments
Nucleotide and arachidonic acid reconstitution experiments were performed using an isotonic-to-isotonic E3 shifting methodology. Laser wounded, anesthetized 2.5–3-dpf larvae expressing AKT-PH-mKate2 mosaically in the basal cells were mounted in 1% low-melting-point agarose in Iso$_{NaCl}$ E3 medium (10–200 µl). A small drop of Iso$_{NaCl}$ E3 medium was placed on the mounted sample to facilitate contact with the water dipping objective lens. At the indicated time after wounding, a bolus (~10× of agarose volume) of Iso$_{NaCl}$-E3 supplemented with 5 mM of the indicated nucleotides/nucleotide-analogues, or 10 µM arachidonic acid, was added to the dish, and responses were imaged for the indicated time using a laser spinning disk confocal microscope (see "Confocal imaging and laser wounding"). As a control for contaminants in the ATP preparation resulting in motility, 5 mM ATP (in isotonic E3) was treated with 5 U/ml apyrase for 2–2.5 h at 28°C before adding to samples.

Statistics
Experiments were performed on at least *n* = 3 independent larvae, unless otherwise indicated. Error bars represent SEM. P-values were derived from unpaired, two-tailed *t* tests.

Online supplemental material
Fig. S1 shows the epidermal layer-specific labeling strategies, the visualization of distinct morphological mechanisms of wound closure in the bilayered epidermis (basal cell lamellipodial migration and suprabasal actin purse-string enrichment), and the effect of tonicity on basal cell migration. Fig. S2 shows the effects of actin and Rho kinase inhibition on wound closure, and the influence of basal epidermal cell migration on the suprabasal layer and wound closure. Fig. S3 demonstrates the effect of tonicity on firefly luminescence. Fig. S4 shows RT-PCR data derived from sorted basal epidermal cells, indicating that *entpd3* is the most prominent ENTPDase in the epidermis, and demonstrates the effects of the splice-blocking *entpd3* MO2 knockdown on tissue motion. Fig. S5 shows that UTP, like ATP, can

reconstitute migration in isotonic medium, but a nonselective P2Y receptor inhibitor, Suramin, fails to inhibit wound closure. Table S1 indicates the pharmacological agonist profile of known P2 receptors. Video 1 shows wound closure in tail fins laser-wounded in hypotonic, isotonic (NaCl), and isotonic (sucrose) media. Video 2 shows that isotonic inhibition of wound closure can be reversed upon hypotonic shifting. Video 3 shows that isotonic medium prevents barrier reconstitution, as visualized by the detection of exogenously added H$_2$O$_2$ by the genetically expressed HyPer sensor. Video 4 demonstrates the simultaneous yet morphologically diverse wound responses present between the basal and suprabasal epidermal layers. Video 5 shows the effect of Rho kinase inhibition on wound closure–associated tissue movement. Video 6 shows that arachidonic acid (AA) fails to reconstitute basal cell migration in isotonic medium. Video 7 shows the nonlytic release of endogenous ATP from a wounded tail fin after exposure to hypotonic medium by means of luciferase-luciferin based luminescence. Video 8 demonstrates enhanced basal cell migration in the presence of an ENTPDases inhibitor (POM 7) and the pan ecto-NTPase inhibitor ATPγS. Video 9 shows that ATP, but not stabilized ATP or ATP metabolites, can reconstitute basal cell migration in isotonic medium. Video 10 shows that UTP, but not stabilized UTP or UTP metabolites, can reconstitute basal cell migration in isotonic medium. Online supplemental material is available at http://www.jcb.org/cgi/content/full/jcb.201408049/DC1.

References

Abreu-Blanco, M.T., J.M. Verboon, and S.M. Parkhurst. 2011. Cell wound repair in *Drosophila* occurs through three distinct phases of membrane and cytoskeletal remodeling. *J. Cell Biol.* 193:455–464. http://dx.doi.org/10.1083/jcb.201011018

Beach, J.R., L.S. Licate, J.F. Crish, and T.T. Egelhoff. 2011. Analysis of the role of Ser1/Ser2/Thr9 phosphorylation on myosin II assembly and function in live cells. *BMC Cell Biol.* 12:52. http://dx.doi.org/10.1186/1471-2121-12-52

Beis, I., and E.A. Newsholme. 1975. The contents of adenine nucleotides, phosphagens and some glycolytic intermediates in resting muscles from vertebrates and invertebrates. *Biochem. J.* 152:23–32.

Belousov, V.V., A.F. Fradkov, K.A. Lukyanov, D.B. Staroverov, K.S. Shakhbazov, A.V. Terskikh, and S. Lukyanov. 2006. Genetically encoded fluorescent indicator for intracellular hydrogen peroxide. *Nat. Methods*. 3:281–286. http://dx.doi.org/10.1038/nmeth866

Bement, W.M., P. Forscher, and M.S. Mooseker. 1993. A novel cytoskeletal structure involved in purse string wound closure and cell polarity maintenance. *J. Cell Biol.* 121:565–578. http://dx.doi.org/10.1083/jcb.121.3.565

Bertrand, J.Y., A.D. Kim, E.P. Violette, D.L. Stachura, J.L. Cisson, and D. Traver. 2007. Definitive hematopoiesis initiates through a committed erythromyeloid progenitor in the zebrafish embryo. *Development*. 134:4147–4156. http://dx.doi.org/10.1242/dev.012385

Block, E.R., and J.K. Klarlund. 2008. Wounding sheets of epithelial cells activates the epidermal growth factor receptor through distinct short- and long-range mechanisms. *Mol. Biol. Cell*. 19:4909–4917. http://dx.doi.org/10.1091/mbc.E08-01-0097

Boucher, I., C. Rich, A. Lee, M. Marcincin, and V. Trinkaus-Randall. 2010. The P2Y2 receptor mediates the epithelial injury response and cell migration. *Am. J. Physiol. Cell Physiol.* 299:C411–C421. http://dx.doi.org/10.1152/ajpcell.00100.2009

Burkel, B.M., G. von Dassow, and W.M. Bement. 2007. Versatile fluorescent probes for actin filaments based on the actin-binding domain of utrophin. *Cell Motil. Cytoskeleton*. 64:822–832. http://dx.doi.org/10.1002/cm.20226

Choi, J., K. Tanaka, Y. Cao, Y. Qi, J. Qiu, Y. Liang, S.Y. Lee, and G. Stacey. 2014. Identification of a plant receptor for extracellular ATP. *Science.* 343:290–294. http://dx.doi.org/10.1126/science.343.6168.290

Enyedi, B., and P. Niethammer. 2013. H2O2: a chemoattractant? *Methods Enzymol.* 528:237–255. http://dx.doi.org/10.1016/B978-0-12-405881-1.00014-8

Enyedi, B., S. Kala, T. Nikolich-Zugich, and P. Niethammer. 2013. Tissue damage detection by osmotic surveillance. *Nat. Cell Biol.* 15:1123–1130. http://dx.doi.org/10.1038/ncb2818

Fuchigami, T., T. Matsuzaki, and S. Ihara. 2011. Exposure to external environment of low ion concentrations is the trigger for rapid wound closure in *Xenopus laevis* embryos. *Zoolog. Sci.* 28:633–641. http://dx.doi.org/10.2108/zsj.28.633

Geiger, J.A., L. Carvalho, I. Campos, A.C. Santos, and A. Jacinto. 2011. Hole-in-one mutant phenotypes link EGFR/ERK signaling to epithelial tissue repair in *Drosophila*. *PLoS ONE*. 6:e28349. http://dx.doi.org/10.1371/journal.pone.0028349

Goldfarb, A.J. 1907. Factors in the regeneration of a compound hydroid, *Eudendrium ramosum*. *J. Exp. Zool.* 4:317–356. http://dx.doi.org/10.1002/jez.1400040302

Goldfarb, A.J. 1914. Changes in salinity and their effects upon the regeneration of *Cassiopea xamachana*. *In* Papers from the Tortugas laboratory of the Carnegie Instiutiton of Washington. Vol. 6. D. Harold, editor. Carnegie Institution of Washington, Washington, D.C. 83–94.

Gong, Z., B. Ju, X. Wang, J. He, H. Wan, P.M. Sudha, and T. Yan. 2002. Green fluorescent protein expression in germ-line transmitted transgenic zebrafish under a stratified epithelial promoter from keratin8. *Dev. Dyn.* 223:204–215. http://dx.doi.org/10.1002/dvdy.10051

Higashijima, S., H. Okamoto, N. Ueno, Y. Hotta, and G. Eguchi. 1997. High-frequency generation of transgenic zebrafish which reliably express GFP in whole muscles or the whole body by using promoters of zebrafish origin. *Dev. Biol.* 192:289–299. http://dx.doi.org/10.1006/dbio.1997.8779

Hoffmann, E.K., I.H. Lambert, and S.F. Pedersen. 2009. Physiology of cell volume regulation in vertebrates. *Physiol. Rev.* 89:193–277. http://dx.doi.org/10.1152/physrev.00037.2007

Huttenlocher, A., and M.C. Poznansky. 2008. Reverse leukocyte migration can be attractive or repulsive. *Trends Cell Biol.* 18:298–306. http://dx.doi.org/10.1016/j.tcb.2008.04.001

Johnson, R.G., Jr. 1988. Accumulation of biological amines into chromaffin granules: a model for hormone and neurotransmitter transport. *Physiol. Rev.* 68:232–307.

Kwan, K.M., E. Fujimoto, C. Grabher, B.D. Mangum, M.E. Hardy, D.S. Campbell, J.M. Parant, H.J. Yost, J.P. Kanki, and C.-B. Chien. 2007. The Tol2kit: a multisite gateway-based construction kit for Tol2 transposon transgenesis constructs. *Dev. Dyn.* 236:3088–3099. http://dx.doi.org/10.1002/dvdy.21343

Kwon, Y., T. Hofmann, and C. Montell. 2007. Integration of phosphoinositide- and calmodulin-mediated regulation of TRPC6. *Mol. Cell*. 25:491–503. http://dx.doi.org/10.1016/j.molcel.2007.01.021

Lavoie, E.G., B.D. Gulbransen, M. Martín-Satué, E. Aliagas, K.A. Sharkey, and J. Sévigny. 2011. Ectonucleotidases in the digestive system: focus on NTPDase3 localization. *Am. J. Physiol. Gastrointest. Liver Physiol.* 300:G608–G620. http://dx.doi.org/10.1152/ajpgi.00207.2010

Lazarowski, E.R., L. Homolya, R.C. Boucher, and T.K. Harden. 1997. Identification of an ecto-nucleoside diphosphokinase and its contribution to interconversion of P2 receptor agonists. *J. Biol. Chem.* 272:20402–20407. http://dx.doi.org/10.1074/jbc.272.33.20402

Loeb, J. 1891. Organization and growth. Wurtzburg.

Martin, P., and J. Lewis. 1992. Actin cables and epidermal movement in embryonic wound healing. *Nature*. 360:179–183. http://dx.doi.org/10.1038/360179a0

Moyer, J.D., and J.F. Henderson. 1983. Nucleoside triphosphate specificity of firefly luciferase. *Anal. Biochem.* 131:187–189. http://dx.doi.org/10.1016/0003-2697(83)90152-5

Müller, C.E., J. Iqbal, Y. Baqi, H. Zimmermann, A. Röllich, and H. Stephan. 2006. Polyoxometalates—a new class of potent ecto-nucleoside triphosphate diphosphohydrolase (NTPDase) inhibitors. *Bioorg. Med. Chem. Lett.* 16:5943–5947. http://dx.doi.org/10.1016/j.bmcl.2006.09.003

Niethammer, P., C. Grabher, A.T. Look, and T.J. Mitchison. 2009. A tissue-scale gradient of hydrogen peroxide mediates rapid wound detection in zebrafish. *Nature*. 459:996–999. http://dx.doi.org/10.1038/nature08119

Nusslein-Volhard, C., and R. Dahm. 2002. Zebrafish: A Practical Approach. Oxford University Press, Oxford. 322 pp.

Orriss, I.R., G.E. Knight, J.C. Utting, S.E.B. Taylor, G. Burnstock, and T.R. Arnett. 2009. Hypoxia stimulates vesicular ATP release from rat osteoblasts. *J. Cell. Physiol.* 220:155–162. http://dx.doi.org/10.1002/jcp.21745

Orriss, I.R., M.L. Key, M.O.R. Hajjawi, and T.R. Arnett. 2013. Extracellular ATP released by osteoblasts is a key local inhibitor of bone mineralisation. *PLoS ONE*. 8:e69057. http://dx.doi.org/10.1371/journal.pone.0069057

Praetorius, H.A., and J. Leipziger. 2009. ATP release from non-excitable cells. *Purinergic Signal*. 5:433–446. http://dx.doi.org/10.1007/s11302-009-9146-2

Radice, G.P. 1980. Locomotion and cell-substratum contacts of *Xenopus* epidermal cells in vitro and in situ. *J. Cell Sci.* 44:201–223.

Redd, M.J., L. Cooper, W. Wood, B. Stramer, and P. Martin. 2004. Wound healing and inflammation: embryos reveal the way to perfect repair. *Philos. Trans. R. Soc. Lond. B Biol. Sci.* 359:777–784. http://dx.doi.org/10.1098/rstb.2004.1466

Reischauer, S., M.P. Levesque, C. Nüsslein-Volhard, and M. Sonawane. 2009. Lgl2 executes its function as a tumor suppressor by regulating ErbB signaling in the zebrafish epidermis. *PLoS Genet.* 5:e1000720. http://dx.doi.org/10.1371/journal.pgen.1000720

Richardson, R., K. Slanchev, C. Kraus, P. Knyphausen, S. Eming, and M. Hammerschmidt. 2013. Adult zebrafish as a model system for cutaneous wound-healing research. *J. Invest. Dermatol.* 133:1655–1665. http://dx.doi.org/10.1038/jid.2013.16

Rosemberg, D.B., E.P. Rico, A.S. Langoni, J.T. Spinelli, T.C. Pereira, R.D. Dias, D.O. Souza, C.D. Bonan, and M.R. Bogo. 2010. NTPDase family in zebrafish: Nucleotide hydrolysis, molecular identification and gene expression profiles in brain, liver and heart. *Comp. Biochem. Physiol. B Biochem. Mol. Biol.* 155:230–240. http://dx.doi.org/10.1016/j.cbpb.2009.11.005

Schindelin, J., I. Arganda-Carreras, E. Frise, V. Kaynig, M. Longair, T. Pietzsch, S. Preibisch, C. Rueden, S. Saalfeld, B. Schmid, et al. 2012. Fiji: an open-source platform for biological-image analysis. *Nat. Methods*. 9:676–682. http://dx.doi.org/10.1038/nmeth.2019

Sonawane, M., H. Martin-Maischein, H. Schwarz, and C. Nüsslein-Volhard. 2009. Lgl2 and E-cadherin act antagonistically to regulate hemidesmosome formation during epidermal development in zebrafish. *Development*. 136:1231–1240. http://dx.doi.org/10.1242/dev.032508

White, R.M., A. Sessa, C. Burke, T. Bowman, J. LeBlanc, C. Ceol, C. Bourque, M. Dovey, W. Goessling, C.E. Burns, and L.I. Zon. 2008. Transparent adult zebrafish as a tool for in vivo transplantation analysis. *Cell Stem Cell*. 2:183–189. http://dx.doi.org/10.1016/j.stem.2007.11.002

Yin, J., K. Xu, J. Zhang, A. Kumar, and F.-S.X. Yu. 2007. Wound-induced ATP release and EGF receptor activation in epithelial cells. *J. Cell Sci.* 120:815–825. http://dx.doi.org/10.1242/jcs.03389

Zimmermann, H., M. Zebisch, and N. Sträter. 2012. Cellular function and molecular structure of ecto-nucleotidases. *Purinergic Signal*. 8:437–502. http://dx.doi.org/10.1007/s11302-012-9309-4